Discrete element simulations and constitutive modeling of dense granular flows

by

Vidyapati

A thesis submitted to the graduate faculty

in partial fulfillment of the requirements for the degree of

MASTER OF SCIENCE

Major: Mechanical Engineering

Program of Study Committee:
Shankar Subramaniam, Major Professor
Pranav Shrotriya
Monica H. Lamm

Iowa State University

Ames, Iowa

2010

TABLE OF CONTENTS

LIST OF TABLES

LIST OF FIGURES

ACKNOWLEDGEMENTS

I would like to take this opportunity to express my sincere thanks and deep appreciations to those who helped me with various aspects of conducting research and the writing of this thesis. First and foremost, I would like to thank Dr. Shankar Subramaniam for his constant guidance, encouragement, patience and support throughout this research and the writing of this thesis. His towering presence instilled in me the carving to work harder and complete the task timely with sufficient degree of independent study. In addition, he is always accessible and willing to help his students. I feel fortunate enough to be a graduate student in his laboratory.

I would also like to thank my POS committee members for their efforts and contribution to this work: Dr. Pranav Shrotriya and Dr. Monica Lamm.

My special appreciation extend to all my fellow lab mates for their kind support, they made my life comfortable and enjoyable. Thank you for your friendship and essential support.

Finally, I would like to extend love and thanks to my family for their patience and enduring support during my graduate studies at ISU.

ABSTRACT

The aim of this study is to understand and explore the rheology of dense granular flow, in particular the phenomenon of regime transition, using both microscale DEM (discrete element method) simulations and macroscale modeling methods. The rheology of dense sheared granular flow in a Couette device is simulated using DEM. It is found that DEM simulations are capable of capturing the regime transition from quasi–static to intermediate behavior. A constitutive model based on the order parameter (OP) framework is refined, and a linear model with new model coefficients extracted from data of 3D DEM simulations of homogeneously sheared granular flows is proposed. The performance of different constitutive models including the refined OP model is tested in the intermediate regime of granular flows. None of these models captures the correct scaling of shear stress with shear rate in the intermediate regime, leading to the conclusion that further development of constitutive models is needed for dense granular flow in the intermediate regime.

CHAPTER 1. INTRODUCTION

1.1 Background

Granular flows are the fundamental particle systems found in solid processing and Nature. For example, solid processing is a multi-billion dollar industry and it remains a critical part of the pharmaceutical (e.g., capsule, tablet solids), agricultural (e.g., fruit, soil), consumer product (e.g., cereal, detergent), and bioenergy (e.g., biomass, biofuels) industries. Understanding the behavior of granular matter is a topic of active research that continues to yield exciting and often surprising results. Granular flow is important in many applications such as silos geometries in pebble–bed nuclear reactor (Rycroft et al., 2006), and clean coal technologies (Syamlal et al., 2009). Rheology of granular flows remains difficult to predict in both Nature and technological application (Fenistein and Hecke, 2003). This is due to the fact that the granular flows exhibit highly complex nonlinear behavior that typically depends on both, the external applied forces as well as, on the internal state of the system.

Modeling the rheology of granular flows using a continuum model is challenging for many reasons: granular flows are strongly dissipative systems far from equilibrium. When densely packed they form force chains, exhibit jamming, stick–slip and phase transition phenomena. These phenomena have been focus of many studies in recent years (Jaeger and Nagel, 1992; Mueth et al., 1998). From an engineering perspective, one of the most interesting phenomena in granular flow is the regime transition from quasi–static to rapid flow regime. This phenomenon of regime transition has been observed in

many industrial and practical applications such as discharge of granular particles from silos or hoppers. However, the mechanisms of regime transition have not been fully understood in spite of many studies in both engineering and physics communities.

Regime transition is governed by a combination of mechanisms, which themselves depend on particle and flow properties. For example, particle properties which influence the regime transition in granular flows are, particle–particle friction coefficient, particle inelasticity and shape of the particle. The flow property which influence the regime transition is shear rate. Figure 1.1 shows the regime map for granular flows with their corresponding constitutive behavior in each regime. As seen in Fig. 1.1, the kinetic theory for rapid granular flow (inertial regime) (Goldhirsch, 2003) predicts a constitutive behavior in which the characteristic scale of stress increases as the square of the strain rate. In the other extreme regime, plasticity models applied to soil mechanics for slow quasi–static flow (Nedderman, 1992; Schaeffer, 1987) result in a stress that is independent of the applied shear rate, and this is confirmed by DEM simulations (Campbell, 2002). However, experiments performed by Tardos et al. (2003) reveal the existence of a third intermediate (transitional) regime that is characterized by $\sigma \propto \dot{\gamma}^n$, where $0 < n < 2$. These experiments also indicate that the intermediate regime is broad enough in the parameter space of solid volume fraction and shear rate to require a continuum model to capture its constitutive behavior.

The current research is focused on the difficulty arising from the existence of different regimes that depends on the nature of grain contacts and applied shear rate. In the quasi–static regime, slowly sheared granular assemblies with enduring frictional contacts between the grains behave like a solid, exhibiting constitutive behavior analogous to plasticity. However, granular material can also behave like a liquid when poured from a hopper or silo, or like a gas when rapidly sheared with the grains experiencing binary, instantaneous collisions at sufficiently low solid volume fraction (Jaeger et al., 1996).

The importance of understanding the regime transition in granular flows and model-

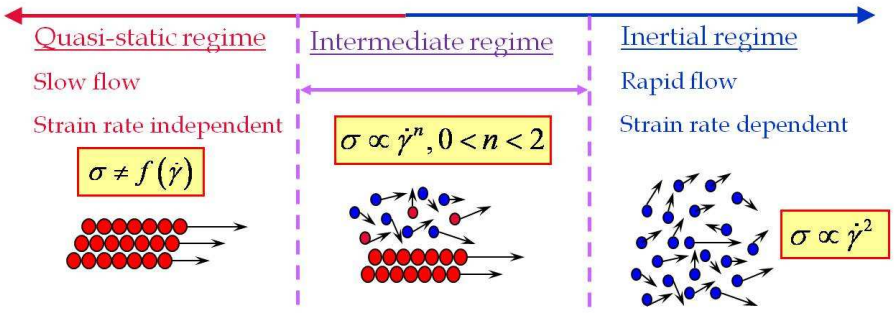

Figure 1.1 Regime map for granular flows and their corresponding constitutive behavior.

ing it accurately, motivates the current research to characterize the constitutive behavior of granular flow in different regimes. The continuum models can be then used in Computational Fluid Dynamics (CFD) tools to better capture the regime transition, and to assist in design and optimization of processes involving granular flows in the intermediate regime.

1.2 Research objectives and approaches

This study addresses the following questions:

1. Are DEM (discrete element method) simulations capable of capturing the regime transition in granular rheology that is observed in experiments?

2. How to incorporate the nature of grain contacts (enduring or instantaneous) into a constitutive modeling framework?

3. How successful are constitutive models in predicting constitutive behavior in different regimes of granular flow?

At the microscale level, the discrete element method (DEM) is employed to simulate dry granular flows. Dry granular flow means absence of cohesive forces in a granular

system. DEM simulates individual particle dynamics and computes the contact forces between particles based on a contact mechanics model. This microscale information will give physical insights into collective particle behaviors, such as flow and microstructure formation, and will guide the continuum model development. Microscale simulations can also be used to validate continuum models. The main goal of this research is to investigate the solid particle behavior from the microscale and incorporate more relevant modeling information into a continuum model at the macroscale.

1.3 Report outline

Chapter 2 provides some background information about continuum modeling and DEM simulations of dense granular flows. Chapter 3 presents a comparison between DEM and experimental study of dense granular flow in a Couette shear cell device. It will be shown that DEM simulations are useful tool to qualitative predict the regime transition in the granular flows, however there are quantitative differences in the predictions. In chapter 4, a linear order parameter (OP) based continuum model is proposed and assessed in the different regimes of granular flows. Chapter 5 summaries the main conclusions from the research work in this study. Possible extensions of this work are discussed from the microscale and macroscale modeling perspectives.

CHAPTER 2. RHEOLOGY OF DENSE GRANULAR FLOWS

This chapter presents a review of existing theories and continuum models for predicting the behavior of dense granular flows. A survey on the role of DEM (discrete element method) simulations in understanding the regime transition in granular flows is also discussed. The focus here is on dense granular flows, because many common materials such as sand require such large shear rates to reach the rapid flow regime that is unattainable for all practical purposes; such material will demonstrate either slow flow or a quasi–static regime behavior depending upon the solid volume fraction.

2.1 Macroscale (continuum) modeling of dense granular flows

A quantitative description of the macroscale behavior of granular flow in industrial devices requires a reliable continuum model. However, even a seemingly simple practical device for the storage and discharge of granular material such as a flat–bottomed silo poses a surprisingly difficult challenge for continuum models (Srivastava and Sundaresan, 2003). Figure 2.1(b) shows that the average vertical discharge velocity from continuum simulations deviates considerably from DEM (discrete element method) simulation data. Granular materials can behave like solids, liquids or gases depending on solid volume fraction, material properties and external forcing conditions (Jaeger et al., 1996). In the quasi–static regime, the majority of external force is supported by force chains within the granular material. For a constant volume simulation, as the shear rate increases,

the force chains become intermittent, being continuously destroyed and regenerated by relative particle motion. As the shear rate increases further, the particle motion becomes more agitated, and the external load is supported by the impact momentum transfer generated when then particle collide with the boundary. This complex behavior makes it very difficult to formulate a comprehensive macroscale theory of granular flow, which can describe all the flow regimes.

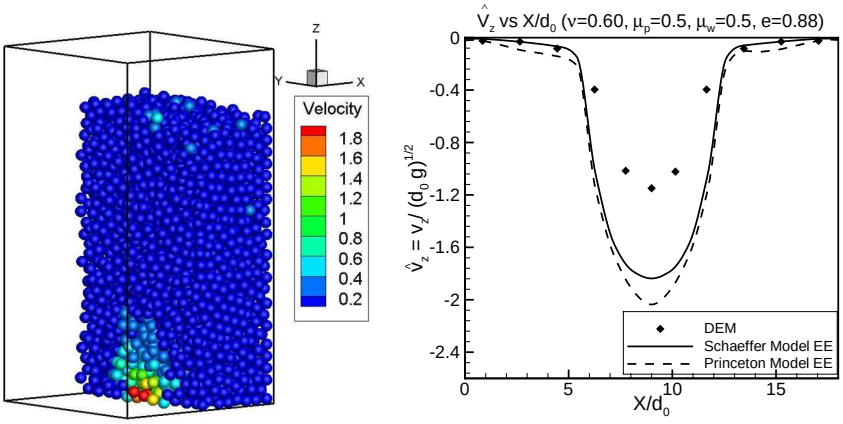

(a) (b)

Figure 2.1 (a) DEM simulation of granular discharge from a flat–bottomed silo with a circular orifice ($d_{orifice}/d_p = 6$), and (b) comparison of the velocity profile obtained using different constitutive relations in an continuum (MFIX, 1993) and DEM simulation.

Approaches to formulate a macroscale model can be classified as:

1. Classical continuum theories.

2. Statistical mechanics (e.g., kinetic theory for granular flows).

3. Micromechanical approach.

4. Phenomenological models based on experiments or computer simulations.

The kinetic theory of granular flow (KTGF) has been reasonably successful in describing the "rapid shear" fluidized regime, whereas the constitutive models based on plasticity

theory perform reasonably well in the dense or quasi–static regime. However, unlike the rapid flow and quasi–static regimes, the intermediate or the transitional regime still lacks a predictive constitutive model even though there have been many studies of granular flow in this regime over the past decades (Jop et al., 2006; GDR MiDi group, 2004). It is clear that a rapid shear granular flow is seldom realized in nature or in industrial process. Even if it does occur, it often coexists with a slow flow or a quasi–static regime. It is extremely difficult to construct theoretical models, which are capable to describe the transition and slow dense flow behaviors. The stress tensor in the granular material is a function of both particle and flow level properties which corresponds to different scales of the problem, e.g., macroscale, meso–scale and microscale. Hence, the granular stress tensor can be represented as,

$$\sigma_{ij} = f(\text{macroscale parameters}, \text{meso–scale parameters}, \text{microscale parameter}). \quad (2.1)$$

Parameters like solid volume fraction and shear rate belong to macroscale in Eq. 2.1. Similarly, interparticle friction coefficient and coefficient of restitution belongs to microscale parameters. The meso–scale parameters can be described by quantities such as the order parameter (OP) and the pair correlation function.

Most of the continuum models (Johnson and Jackson, 1987; Srivastava and Sundaresan, 2003) used to predict the behavior of granular flows are based on an additive decomposition of the total granular stress as a weighted sum of kinetic and frictional contributions ($\sigma_{ij} = \sigma^k_{ij} + \sigma^f_{ij}$), with the weight factor specified solely as a function of the solid volume fraction. Existing models for the particle pressure at the packing limit are inadequate, although a recently proposed model (Sun and Sundaresan, 2010) for granular stress in the quasi–static regime that is based on the evolution of the fabric tensor promises to remedy this deficiency. Both experiments in a 2D granular shear cell (GSC) (McCarthy et al., 2010) and DEM simulations (Volfson et al., 2003) reveal that grain contact in the intermediate regime are in a "phase transition" characterized by a

mix of enduring solidlike contacts and transient fluidlike contacts. While most constitutive models in use are phenomenological, this observation motivates the development of a constitutive model for the intermediate regime based on microscale physical interactions between the grains. In particular, these grains interactions are not determined by the solid volume fraction alone, but are dependent on particle properties (such as particle friction coefficient, inelasticity) and the local shear rate. Consequently, the simple additive models are not capable of capturing this complex constitutive behavior, these models also assume that the stress and strain rate are coaxial (Savage, 1998), but this assumption is not verified in the intermediate regime.

Savage (1998) proposed a continuum theory based on associated flow rule that relates the strain rate and the shear stress in plastic frictional systems. Averaging strain rate fluctuations yields a Bingham–like constitutive relation, in which the shear stress and strain rate tensors are always coaxial. Furthermore, it also postulates that the viscosity diverges as the density approaches the close–packing limit. The problem of slow granular flow in rough–walled vertical chute was studied by this model. A concentration boundary layer being thicker than the velocity boundary layer was obtained, which was consistent with the experimental observations.

Aranson and co–workers (Aranson and Tsimring, 2002; Volfson et al., 2003) proposed an alternative additive model that attempts to characterize the granular "phase transition" in the intermediate regime using an approach analogous to the Landau theory of phase transitions (Landua and Lifshittz, 1980) by introducing a scalar order parameter, that is used to determine, the relative contribution of kinetic and frictional stresses. The order parameter (OP) is defined as the ratio of space–times averaged number of "solid" contacts to all contacts within a sampling volume,

$$\rho = \frac{\overline{\langle Z_s \rangle}}{\overline{\langle Z \rangle}}. \tag{2.2}$$

The stress was decomposed into a "fluid" and "static" part,

$$\sigma_{ij} = \sigma_{ij}^{f} + \sigma_{ij}^{s}. \tag{2.3}$$

The value of the order parameter specifies the ratio between the static and fluid part of the stress tensor. The order parameter was assumed to obey dissipative dynamics governed by a free energy functional with two local minima. This description was based on the separation of static and fluid components of the shear stress and assumed Newtonian friction law for the fluid components. The viscosity coefficient is expected to remain finite at the fluidization threshold. This model yields a good qualitative description of many phenomena occurring in granular flows. However, the model is limited to two dimensions and the correlation of the order parameter with the model coefficients was fitted from only 2D molecular simulations. The stress tensor in this model was correctly generalized to an objective form that is independent of the coordinate system by Gao et al. (2005). This objective representation correctly models the isotropic and anisotropic parts of the stress tensor. This general objective form of the model also relaxes the assumption in the original model that the principal axes of the granular stress tensor be coaxial with that of the fluid stress tensor.

2.2 Microscale (discrete) modeling of granular flows

Microscale models of granular flow treat the granular material as a collection of discrete particles and resolve particle interactions at the scale of individual particles. A contact mechanics model is used in an molecular dynamics (MD) algorithm to capture multiparticle contacts. Design of a molecular dynamics simulations should account for the available computational power. Simulation size (n = number of particles), time step and total time duration must be selected so that the calculation can finish within a reasonable time period. However, the simulations should be long enough to be relevant to the time scales of natural processes being studied. Generally a cutoff distance r_{cut} is

introduced in potential functions and both potential functions and their gradients beyond the cutoff distance are assumed to be zero. This treatment can reduce the computing time greatly by neglecting all atoms beyond the cutoff distance, since interaction between these atoms are zero and need not to be considered. This procedure scales $O(N^2)$ as the system size.

Microscale simulations can produce useful information to derive macroscopic constitutive relations needed to describe the material within the framework of a macroscale continuum theory. The microscale simulations also serve to validate the continuum models by testing the validation of their underlying assumptions and range of their applications in terms of all the simulation parameters (e.g., particle volume fractions, interparticle friction coefficients, shear rates etc.). There basically exist two different approaches, the so–called soft sphere DEM (discrete element method) and the hard sphere, event–driven method. The former is straightforward, easy to generalize, and has numerous applications, while the latter is optimized for rigid interactions and is mainly used for collisional, dissipative granular gases where only binary collisions are important. The idea of DEM is to numerically integrate the equations of motion for all the particles in the system (Allen and Tildesley, 1989). Soft sphere DEM for granular flows is to supply contact force models for solid particles. Pioneering work in this field was done by Cundall and Strack (1979). Since the realistic modeling of the deformations of the particles is such too complicated, a simplified contact force and the overlap relation (Silbert et al., 2001), the so called spring–dashpot model, is used in this work which is shown in Fig. 2.2.

DEM has been successfully used to quantify the constitutive behavior of granular flow in different regimes (Campbell, 2002; Aarons and Sundaresan, 2006). A quantitative understanding of the different regimes of flow for monodisperse, cohesionless, frictional particles has emerged from DEM simulations performed by Campbell (2002). Using DEM simulations of homogeneously sheared flow of cohesionless particles in periodic

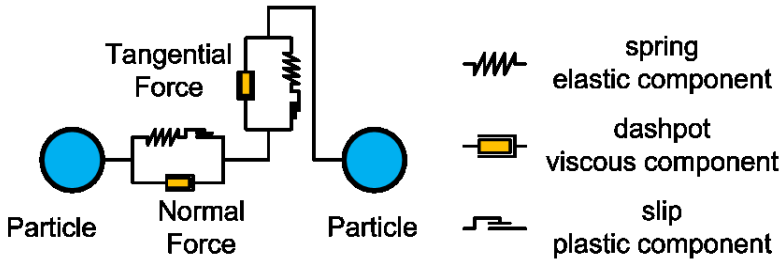

Figure 2.2 Standard contact law in DEM.

domains Campbell (2002) identified different regimes of granular flow mainly inertial (rapid flow), quasi–static and an intermediate. Campbell (2002) confirmed that DEM reproduces the qualitative constitutive behavior that is observed in the experiments namely, that in the inertial regime stress increases as the square of the strain rate, in the elastic quasi–static regime the stress did not vary appreciably with the applied shear rate, and in the intermediate regime the stress varies with the applied shear rate, but this relation takes different forms that depends on the solid volume fraction, interparticle friction coefficient and shear rate.

Aarons and Sundaresan (2006) performed DEM simulations of cohesive particles in order to investigate the effect of interparticle attractive forces on the regime of rheology manifested by dense assemblies. They (Aarons and Sundaresan, 2006) showed that with the addition of interparticle attractive forces the regime boundaries shift in a systematic manner, and that the quasi–static regime expands. McCarthy et al. (2010) used detailed particle level experimental measurements to quantitatively validate DEM simulations in an annular shear cell. The velocity, granular temperature and solid volume fraction profiles was extracted by using particle tracking velocimetry (DPIV) and compared with the computational data. They also studies the influence of the contact mechanics model and performed sensitivity analysis on device and particle geometry and material properties employed. In a recent work by Vidyapati et al. (2010), the rheology of dense granular

material is studied using an annular Couette cell by experiments and computations. It is shown that DEM simulations are capable of capturing the regime transition from quasi–static to intermediate regime when a secondary vertical flow is induced, which is also observed in the experiments. Ketterhagen et al. (2009) used DEM to assess powder flow from hoppers and results were compared to widely used hopper design charts. A Mass Flow Index (MFI) based on velocity profile data is used to quantitatively characterize the nature of the flow pattern as mass–flow, funnel–flow or some intermediate.

2.3 Summary

In this chapter, the fundamental microscale and macroscale methods for modeling granular flows have been reviewed with emphasis on the capability to capture the regime transition in the granular flows. As discussed in Eq. 2.1, existing constitutive models for granular flow should take into account the different parameters at different scales, e.g., macroscale, meso–scale and microscale. However, it is found that most of the continuum models for granular flow take into account the parameters which belongs to, two extreme scales (macroscale and microscale) of the problem. Nevertheless very few model (such as OP model proposed by Volfson et al. (2003)) take into account the intermediate scale (meso–scale) of the problem in the framework of a constitutive model. This review also guides the research to determine the capabilities and limitations of the state–of–art models and to contribute to the new understanding and development of continuum models.

CHAPTER 3. EXPERIMENTAL AND COMPUTATIONAL STUDIES OF DENSE GRANULAR FLOW: TRANSITION FROM QUASI–STATIC TO INTERMEDIATE REGIME IN A COUETTE SHEAR DEVICE

This chapter is a manuscript submitted to Powder Technology, titled "Experimental and computational studies of dense granular flow: transition from quasi–static to intermediate regime in a Couette shear device" authored by Vidyapati, M. Kheiripour, J. Sun, S. Sundaresan, G.I. Tardos and S. Subramaniam.

Abstract

Rheology of dense granular material is studied using an annular Couette cell by experiment and computation. A transition from quasi-static to intermediate behavior is identified when a secondary vertical flow is induced. This secondary-flow-induced transition and a power-law relation between stress and strain rate in the intermediate regime are verified to be robust rheological features by simulation using discrete element method (DEM). The insensitivity of this transition and the relation to certain particle and operational parameters is also shown by the simulation. The transitional and intermediate behavior is modeled by an order parameter (OP) based model with the fluidlike stress supplied from the original kinetic theory for granular flows (KTGF). The suitability of this approach is discussed.

Notation for section 3.1 to section 3.5

d_0 particle diameter

$\triangle t$ time step for simulation

e particle restitution coefficient

F_0 scaling factor for force

F_n normal force

F_t tangential force

g acceleration due to gravity

k^* nondimensional shear rate

k_0 scaling factor for stiffness

k_n particle normal stiffness coefficient

k_t particle tangential stiffness coefficient

m_0 particle mass

t time

t^* typical time of collisional for solid contacts

t_0 scaling factor for time

t_c binary collision time

v velocity

v_0 scaling factor for velocity

Z total number of contacts

Z_s number of solid contacts

Greek symbols

$\dot{\gamma}$ shear rate

$\dot{\gamma}_{max}$ maximum shear rate

γ_n particle normal damping coefficient

γ_t particle tangential damping coefficient

$\hat{\gamma}$ nondimensional shear rate based on gravity scaling

μ_p particle friction coefficient

μ_w wall friction coefficient

ν solid volume fraction

ρ particle density

σ_0 scaling factor for stress

σ_{ij} total granular stress

σ_{ij}^f fluidlike contribution to the total granular stress

σ_{ij}^s solidlike contribution to the total granular stress

σ_{yx} shear stress

σ_{yy} normal stress

3.1 Introduction

Granular materials could mimic the behavior of solid, liquid or gas (Jaeger et al., 1996) subject different exiting conditions. Understanding this complex behavior poses challenging scientific questions and is also of practical importance to many industrial processes, such as silo discharge, chute flow and dense-phase pneumatic (Sundaresan, 2001). Many experimental work has been performed to probe the diverse behavior of granular materials. As classical examples, (Reynolds, 1885) examined dilatancy behavior of quasi-statically deformed granular assemblies and (Bagnolds, 1954) studied the inertial behavior and proposed the quadratic dependence of stress on shear rate. However, the transition from quasi-static to inertial regime and the intermediate behavior in between are even more fascinating and difficult to quantify. This paper presents the transitional and intermediate behavior observed in our experiments and simulations and addresses continuum modeling of the behavior as well.

The experiment technique of choice in this study is using an annular Couette shear cell, which has been adopted from fluid rheology experiment to study granular rheology for some years (Savage and Sayed, 1984; Miller et al., 1996; Tardos et al., 2003; Tsai and Gollub, 2004; GDR MiDi group, 2004). For example, Savage and Sayed (1984) reported shear and normal stress variations with respect to shear rates obtained from an annular shear cell. Velocity profiles in the annulus has also been measured (GDR MiDi group, 2004). In these experiments, however, either the flow behaved in a single regime (GDR MiDi group, 2004) or the transition from quasi-static regime to inertial regime was not explicitly controlled (Savage and Sayed, 1984). To facilitate control of flow regime transition, a modified Couette cell was devised in this study to have a hopper connected to the bottom of the cylindrical cell. A secondary vertical flow can thus be introduced to granular material in the annulus by discharge from the hopper. It will be shown that the transition can be triggered by the onset of this secondary flow. The

stress and shear rate relation for intermediate flow behavior will also be presented.

Discrete element method (DEM) (Cundall and Strack, 1979) simulation has been used extensively to simulate Couette shear flow. Simulations have been performed to study a two-dimensional (2D) Couette cell for photoelastic disks and found reasonable agreement with the corresponding experimental result on the velocity profile (Schöllmann, 1999). Similar 2D simulations also produced variation of pressure versus volume fraction that was consistent with experiments (Majmudar et al., 2007). In this paper, DEM simulations in a simplified three-dimensional (3D) domain have been set up to study the essential flow characteristics probed by the modified Couette cell experiments. The results will verify the transitional and intermediate behavior observed in the experiments and further demonstrate the robustness of these trends against variations in some particle level properties. They also provide necessary micromechanical parameters as input for an order parameter (OP) model.

The OP model was initially proposed by Volfson et al. (2003), in which total stress is decomposed into solidlike and fluidlike parts and the ratio between them is specified by an OP. A generalized version of this model (Gao et al., 2005) was further linearized and employed to study the intermediate behavior in this paper. The definition of solidlike or fluidlike stress is based on whether the involved particle contacts are enduring. This micromechanics based approach provides an alternative to the directly-additive stress approach proposed by Savage (1983, 1998), in which inertial stress calculated according to the kinetic theory for granular flows (KTGF) (Goldhirsch, 2003) is directly added to the quasi-static stress from soil mechanics theories (Nedderman, 1992). However, it will be shown that simply adopting KTGF for fluidlike stress in the OP model cannot lead to a correct prediction of the intermediate behavior.

3.2 Couette cell experiment and simulation details

Granular shearing experiments were performed in a modified annular Couette cell as shown in the schematic diagram in Fig. 3.1. The device consists of a cylindrical portion with a rotating inner cylinder to shear the material in the annular gap and a conical hopper at bottom. The material above the rotating cylinder (denoted as overburden in the schematic) is stationary and provides dead weight to the sheared layer. Granular material can be fed from above using a vibrating feeder (not shown) and discharged by a screw-in-cylinder metering device (also not shown) that discharges the material and allows for precise flow rate measurement. For experiments operated in a continuous mode, material is fed and discharged at the same time to achieve a steady state vertical flow in the sheared layer. For experiments in a batch mode, no mass flows in or out of the device. Shear stresses can be measured indirectly from the torque on the rotating cylinder. DEM simulations were carried out to verify experimental findings

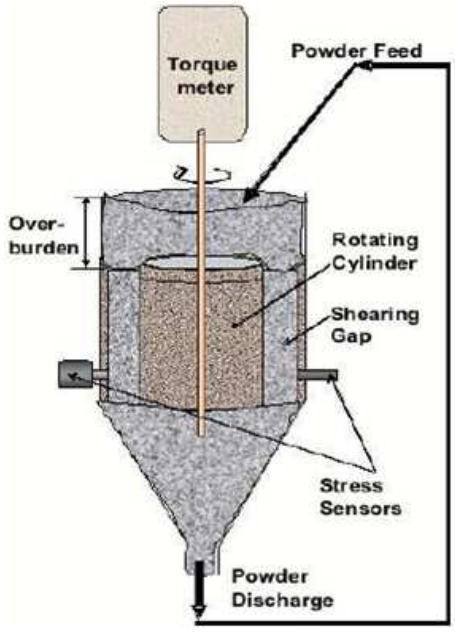

Figure 3.1 Schematic representation of axial–flow Couette device.

and to further study parametric dependence of the granular rheology. The simulations were performed in three dimensions (3D) using monodisperse, non–cohesive spheres of diameter d_0 and mass m_0, under the influence of gravity g. A soft sphere model was used, in which particles interact via contact laws and friction only on contact. Since the realistic modeling of particle deformation is complicated, a simplified contact force and the overlap relation (Silbert et al., 2001), the linear spring–dashpot model, was used in this work. A nondimensional system of equations is solved, where the scaling factor for distance, time, velocity, force, elastic constants and stresses are d_0, $t_0 = \sqrt{d_0/g}$, $v_0 = \sqrt{gd_0}$, $F_0 = m_0 g$, $k_0 = m_0 g/d_0$ and $\sigma_0 = m_0 g/d_0^2$, respectively. As the problem involves both shear and gravity effects, two different kinds of scaling could be used to nondimensionalize the input parameters. Table 3.1 shows the different computational parameters with their corresponding gravity and shear based scaling. The selection of correct scaling for the simulation was determined from the limiting time scale involved in the problem, which was found to be based on gravity. Details of the computational model used in the discrete element simulations are given in Appendix A, and additional details can be found in Silbert et al. (2001), and Sun et al. (2006).

Table 3.1 Scaling for different computational parameters.

Parameters	Gravity Scaling	Shear Scaling
Length, L_0	d_0	d_0
Time, t_0	$\sqrt{d_0/g}$	$1/\dot{\gamma}$
Velocity, v_0	$\sqrt{gd_0}$	$d_0\dot{\gamma}$
Force, F_0	$m_0 g$	$m_0 d_0 \dot{\gamma}^2$
Stiffness, k_0	$m_0 g/d_0$	$m_0\dot{\gamma}^2$
Stress, σ_0	$m_0 g/d_0^2$	$m_0\dot{\gamma}^2/d_0$
Damping Coefficient, γ_n	$m_0\sqrt{g/d_0}$	$m_0\dot{\gamma}$

The total number of particles in the whole experimental system, including those in the overburden and hopper, is extremely large for DEM simulation. To avoid this expensive

simulation, but still capture the essential rheological behavior, a representative slice of the sheared the granular layer was simulated. The curvature of the layer was also ignored due to the relatively large cylinder diameter, and a cubical domain as shown in Fig. 3.2 was used. The side of the cube selected was $14d_0$. The effect of control volume size was tested by examining cubical control volumes ranging in size from $7d_0 \times 7d_0 \times 7d_0$ to $20d_0 \times 20d_0 \times 20d_0$. No effect was found on the resultant stress as long as side of the cube selected was at least $10d_0$. A similar study was performed by Campbell (2002), where he showed that the resultant stress remains unchanged as long as the dimensions were at least $7d_0 \times 7d_0 \times 7d_0$. To account for the downward motion of the granular material in

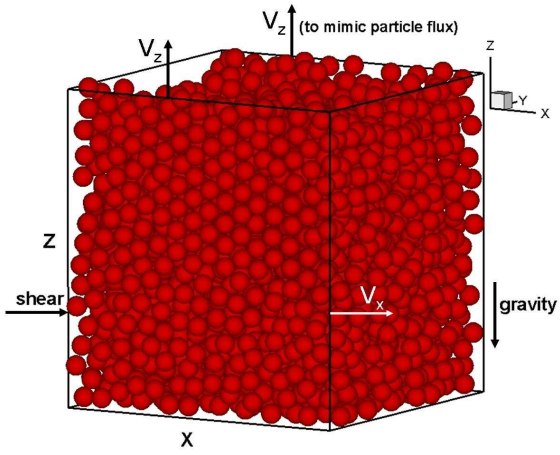

Figure 3.2 The schematic of spherical particles bounded in cubical domain, V_z shows the upward motion of the wall (to mimic particle flux), and V_x shows the direction of shearing.

the Couette cell as in the continuous mode experiments, the walls located at $y = 0$ and at $y = L$ (corresponding to radial co-ordinates in Couette cell), were given a velocity v_z in the positive z direction. To mimic the batch mode operation of the Couette device, v_z was set to zero. The wall located at $y = 0$ was given a velocity v_x in the positive x direction to produce the shearing motion; this velocity was calculated based on the

shear rate used in the experiments. The domain was bounded with periodic boundaries in the x direction (which corresponds to the azimuthal direction in the Couette cell). At $z = 0$, a flat–frictional wall was placed, whereas at $z = L$, the "shrink wrap" boundary condition was used. The shrink wrap boundary condition ensures that the position of the face is set so as to encompass the particles in that dimension, no matter how far they move. All the walls used in the simulations were flat–frictional walls with a friction coefficient of 1.0. Gravity was imposed in the negative z direction to mimic the actual experimental setup.

DEM simulations were performed for three different (0.64, 0.62, 0.60) values of the initial solid volume fractions. As the simulation progresses the solid volume fraction no longer remains uniform but develop spatial inhomogeneities. Shear rates were chosen same as used in the experiments. Some of the parameters that were not available from the experiments were assigned values based on reasonable physical estimation for glass beads of 0.1 mm in diameter used in the experiments. For instance, the normal spring stiffness was assigned to be 2×10^5, which captures the general behavior of intermediate to high k_n systems (Silbert et al., 2001). This gives a reasonable representation of realistic granular materials in some circumstances. Similarly a value of 0.9 was selected for restitution coefficient (Silbert et al., 2001) and a value of 0.19 was selected for particle–particle friction coefficient (which corresponds to friction coefficient of glass beads used in the experiments). Sensitivity of the simulation results to particle parameters was checked to ensure that trends are physically consistent.

The time step $\triangle t$ was selected to be one fiftieth of the binary collision time t_c, which is small enough for a temporally converged numerical simulation (Silbert et al., 2001). Simulations were run to a nondimensional time of $\dot{\gamma}t = 500$, which is long enough to attain a statistically stationary solution (Campbell, 2002). Sensitivity study reveals that stresses increases with initial solid volume fraction, and we present result for a solid volume fraction of 0.64, which are closest to the experiments. The average stress is cal-

culated by dividing the force acting on the inner wall by the granular bed cross sectional area considering its expansion or compaction. Table 3.2 shows the basic computational parameters that are chosen to mimic the experiments as closely as possible.

Table 3.2 Basic computational parameter settings.

Parameters	Values
Number of particles	3348
Particle diameter	d_0
Particle density	$1.91(m_0/d_0^3)$
Particle normal stiffness coefficient, k_n	$2 \times 10^5(k_0)$
Particle tangential stiffness coefficient, k_t	$2/7k_n$
Particle normal damping coefficient, γ_n	$40(1/t_0)$
Particle tangential damping coefficient, γ_t	$0(1/t_0)$
Particle friction coefficient, μ_p	0.19
Particle restitution coefficient, e	0.9
Wall normal stiffness coefficient	$2 \times 10^5(k_0)$
Wall tangential stiffness coefficient	$2/7k_n$
Wall normal damping coefficient	$40(1/t_0)$
Wall tangential damping coefficient	$20(1/t_0)$
Wall friction coefficient, μ_w	1.0
Time step, dt	$1 \times 10^{-4}(t_0)$

3.3 Experimental and simulation results

3.3.1 Transitional and intermediate behavior

Rheological behavior for sheared granular material probed by the Couette cell experiments and simulations is presented in this section. In Fig. 3.3 the average shear stress is plotted against time for batch-mode operation of the Couette device. Figure 3.3 shows that changing the shear rate more than five folds in simulation does not result in any significant change in the shear stress: this rheological behavior corresponds to the quasi–static regime. DEM results show initial fluctuations in the stress level, but attain a statistically stationary condition after approximately 30 nondimensional time

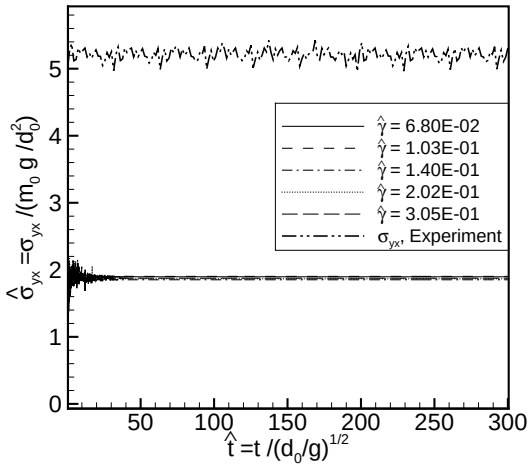

Figure 3.3 Temporal evolution of the average shear stress in batch-mode operation of the Couette device. Simulations parameters: $\nu = 0.64$, $\mu_p = 0.19$, $\mu_w = 1.0$, $e = 0.9$, $v_z = 0.0$ mm/s.

units. Similar behavior was observed in the experiments performed when the Couette device operated in the batch mode. However, the magnitude of the shear stress is about 2.5 times higher than those predicted in the simulations. It should be noted that the experiments were also performed with different values of shear rates, but only one of those was presented in Fig. 3.3 due to their close proximity.

The variation of shear stress with shear rate in the continuous mode of operation with a vertical speed, $v_z = 0.1$ mm/s, is shown in Fig. 3.4 (the left Y axis of Fig. 3.4 corresponds to the DEM simulation results and the right Y axis corresponds to the experimental data). The experimental results in Fig. 3.4 show that the flow exhibits two distinct regimes: a quasi-static regime where the shear stress is independent of the shear rate (at very low shear rates) and an intermediate regime where the dependence takes the form of a power-law. The DEM results show the same trend; however, the magnitude of the shear stress is about 4.5 times lower than its experimental counterpart. A similar study performed by Ji et al. (2009) reported a quantitative discrepancy of

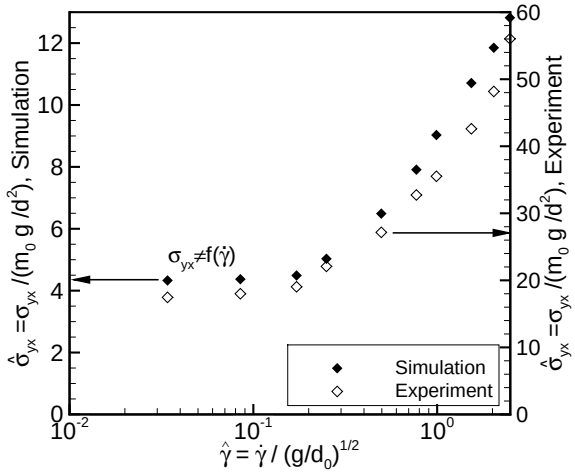

Figure 3.4 Variation of average shear stress with shear rate for continuous mode of operation of Couette device. The filled symbols denote the DEM simulation results, while the open symbols are for data obtained from experiments. The left and right axes are for the DEM and experimental data, respectively, and use different scales to emphasize the similar variation trends between the two cases. Simulations parameters: $\nu = 0.64$, $\mu_p = 0.19$, $\mu_w = 1.0$, $e = 0.9$, $v_z = 0.1$ mm/s.

a factor of two between measured and simulated shear stresses. This difference in the magnitude of the shear stress between experiment and simulation could be due to several reasons, including:

(i) approximations in the particle properties such as coefficient of friction,

(ii) differences in geometry: the DEM simulation was performed with planar walls and the system simulated was smaller than experimental device,

(iii) dependence of stress on the specific contact mechanics model (McCarthy and Higgs, 2009), and

(iv) differences in the solid volume fraction that is not known from the experiment.

In Fig. 3.5, the ratio of shear to normal stress is plotted as a function of shear rate for continuous mode of operation. Since both the experimental and the DEM studies (results not shown here) show that the normal stress is practically independent of the shear rate in the continuous mode of operation, while the shear stress shows a dependence, one would expect that this ratio (σ_{yx}/σ_{yy}) should vary with shear rate. Figure 3.5 shows that this ratio remains almost constant for lower shear rate and approximately equal to the apparent friction coefficient of the glass beads used.

As the dimensionless shear rate increases beyond a certain critical value, this ratio of shear to normal stress increases significantly. Both simulations and experiments show a similar trend but they diverge to slightly different values at lower shear rates. Comparing the stress ratios in Fig. 3.5 with the shear stress in Fig. 3.4 it can be seen that while the experimental shear stress is about 5 times of the simulation results, the stress ratios are much closer (only less than 2 times larger). This comparison shows that the normal stress in experiment is also larger, which is the result of the overburden presented in the experiment but ignored in the simulation.

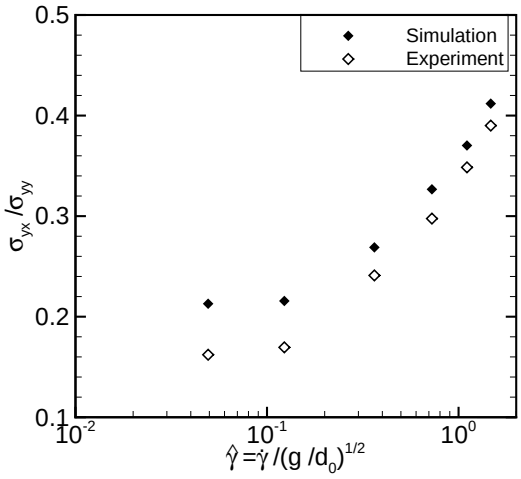

Figure 3.5 Ratio of shear to normal stress as a function of shear rate in continuous mode of operation. Filled symbols corresponds to DEM simulations whereas the open symbols are experiment data. Simulations parameters: $\nu = 0.64$, $\mu_p = 0.19$, $\mu_w = 1.0$, $e = 0.9$, $v_z = 0.1$ mm/s.

3.3.2 Simulation parametric study

As reported earlier, some of the parameters (such as the solid volume fraction, particle stiffness and interparticle friction coefficient) in the DEM simulations that are not available from the experiments were assigned reasonable values. In order to quantify the effect of these parameters on the stress level, we performed a parametric study with different values of solid volume fractions, particle stiffness and wall friction coefficients. These simulations were performed in a same Couette cell setup as discussed in section 3.1.

1. Solid volume fraction: Figure 3.6(a) shows the variation of average shear stress against solid volume fraction. The interparticle and wall friction coefficient were set to 0.2 and 0.5, respectively, for these simulations. As expected the stress level increases with the increase in solid volume fraction. However, we found that this

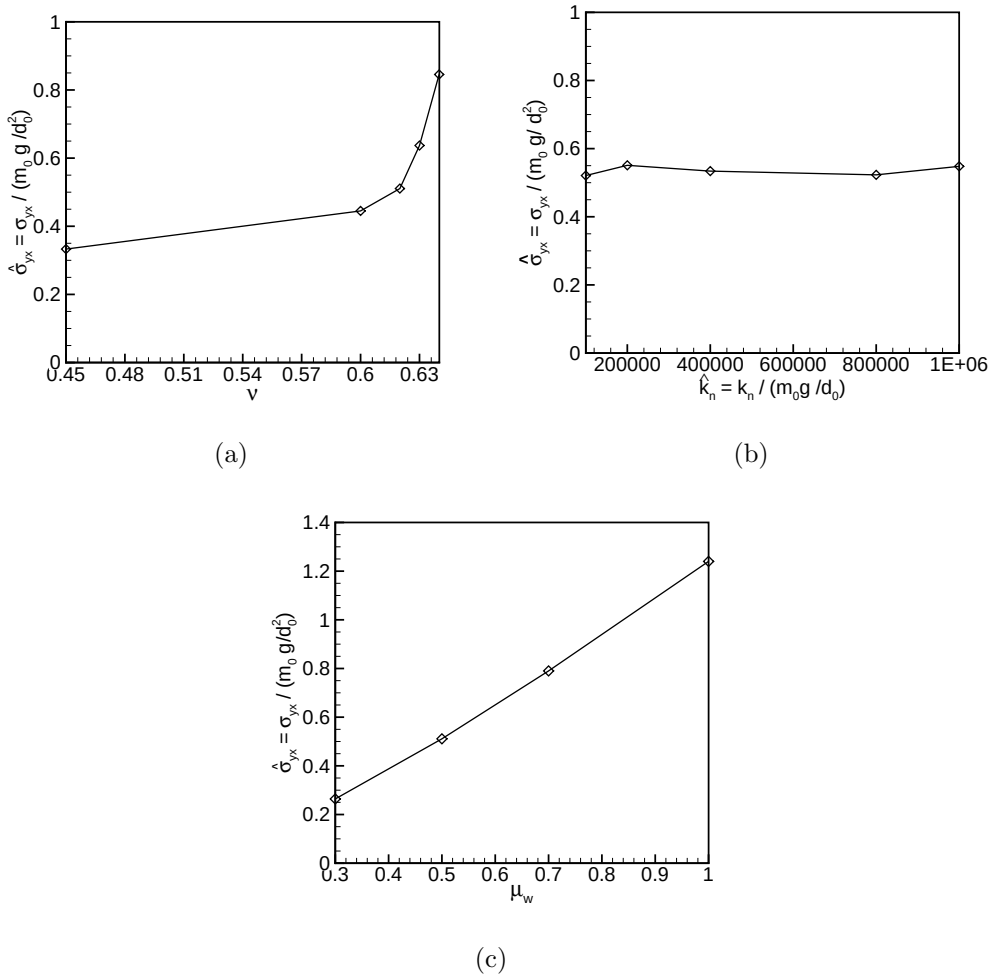

Figure 3.6 (a) Effect of solid volume fraction on the average shear stress. Simulation parameters: $\mu_p = 0.2$, $\mu_w = 0.5$, $e = 0.9$, $v_z = 0.0$ mm/s, (b) Effect of particle stiffness on the average shear stress. Simulation parameters: $\mu_p = 0.2$, $\mu_w = 0.5$, $e = 0.9$, $v_z = 0.0$ mm/s, and (c) Effect of wall friction coefficient on the average shear stress. Simulation parameters: $\nu = 0.62$, $\mu_p = 0.2$, $e = 0.9$, $v_z = 0.0$ mm/s, $\hat{\gamma} = 0.14$.

effect is pronounced in the high solid volume fraction regime (above a solid volume fraction of 0.60), where a non–linear increase in the stress level is seen.

2. Particle stiffness: To assess the effect of particle stiffness on the stress level, we performed DEM simulations with different values of particle stiffness ranging from 10^5 to 10^6. The solid volume fraction used in these simulations is 0.62, with a interparticle friction coefficient of 0.2 and wall friction coefficient of 0.5. As Fig. 3.6(b) shows, there is almost no change in the stress level with particle stiffness. Whereas, in constant volume simulations the stress level increases with increase in the particle stiffness, in the Couette cell simulations the bed is allowed to expand freely which causes the stress level to remain constant, regardless of the different particle stiffness.

3. Wall friction coefficient: In order to investigate the effect of wall friction on the stress level, we performed DEM simulations with different values of wall friction coefficient ranging from 0.3 to 1.0. The solid volume fraction used for these sets of simulations is 0.62, with a interparticle friction coefficient of 0.2. Figure 3.6(c) shows the variation of average shear stress with wall friction coefficient. As expected the stress level increases with increase in the wall friction coefficient. A five-fold increase in the stress level is observed when the wall friction coefficient is increased from 0.3 to 1.0.

To understand the impact of axial velocity of the granular particles in the shear gap, we performed additional simulations (results not presented here) with different axial velocities of 0.0, 0.05, 0.1 and 0.2 mm/s. We found a sudden increase (a factor of two) in the magnitude of the average shear stress when the axial velocity was increased from 0.0 to 0.05 mm/s. However, any further increase in the axial velocity of the granular particles does not result in any appreciable change in the average shear stress magnitude. This increase of the shear stress from batch mode to continuous mode in the simulations

is counterintuitive and could be attributed to the fact that the overburden was ignored in the simulations.

3.4 Order parameter modeling and analysis

The OP model was developed by Aranson, Tsimring and Volfson in a series of papers (Volfson et al., 2003; Aranson and Tsimring, 2002). The fundamental premise of this model is that one can define an OP in granular flows similar to that used in the Landau theory of phase transition. In (Volfson et al., 2003), the OP is defined as the ratio of space-time averaged number of "enduring" contacts $\overline{\langle Z_s \rangle}$ to all contacts $\overline{\langle Z \rangle}$ within a sampling volume. A contact is considered enduring only if it is in a stuck state ($F_t < \mu_t F_n$) and its duration is longer than a typical time of collision t^*, which is generally taken as 1.1 times the binary collision time t_c (Volfson et al., 2003). The first requirement eliminates long lasting sliding contacts, and the second excludes short term collisions. The OP is useful in characterizing two limiting cases: when the granulate is in "solid" state and when it is strongly agitated, i.e., completely fluidized. In the solid state all contacts are enduring and hence OP = 1. In the fluidized case, the number of solid contacts is zero with finite total number of contacts, therefore OP = 0.

The original OP model (Volfson et al., 2003) decomposes the total stress tensor into "solidlike" and "fluidlike" contributions based on the value of the OP. The OP model gives expression for "solidlike" and "fluidlike" stress tensors as functions of OP and the total granular stress tensor σ_{ij}. The original OP model by Volfson et al. (2003) was generalized to an objective form by Gao et al. (2005), which has been refined by extracting the model coefficients from 3D DEM simulations of homogeneously sheared granular flow (see details in Appendix B). The linear version of the objective OP model, denoted as a refined order parameter (ROP) model, was employed in this study. To complete the ROP model specification, it was assumed that the "fluidlike" part of the

total granular stress can be computed form the kinetic theory of granular flow (KTGF) following Aranson and Tsimring (2002) . Then the total granular stress tensor can be expressed in terms of the "fluidlike" stress and the ROP model coefficients. Details of the ROP model can be found in Subramaniam and Vidyapati (2009) and Vidyapati et al. (2010).

In order to investigate the functional dependence of OP, we performed homogeneous shear simulations with four volume fractions and three values of the particle-particle coefficient of friction. Figure 3.7(a) shows that the OP increases as the volume fraction increases and is indeed strongly dependent on the coefficient of friction. An increase of 300% in the values of OP is seen when the coefficient of friction increases from 0.1 to 1.0. This result is expected because the number of "solid" contacts increases with increase in volume fraction and the larger interparticle friction is, the more particles are prevented from sliding over each other.

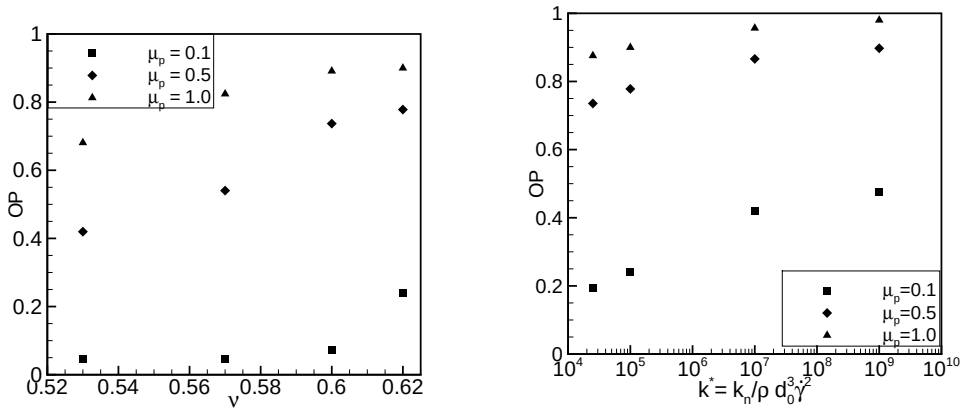

(a) (b)

Figure 3.7 (a) Order parameter as a function of volume fraction for homogeneous shear simulation, simulation parameters: $k^* = 10^5$, $e = 0.7$ and (b) Order parameter as function of shear rate ($k^* = k_n/\rho d^3\dot{\gamma}^2$) for homogeneous shear simulation, simulation parameters: $\nu = 0.62$, $e = 0.7$.

We then ascertain the functional dependence of OP on flow properties such as shear

rate. In Fig. 3.7(b) the OP values are plotted as a function of nondimensional shear rate ($k^* = k_n/\rho d^3\dot{\gamma}^2$) for homogenous shear simulation. As Fig. 3.7(b) shows, the OP value increases with decreasing shear rate, corresponding to an increase in the solid-like enduring contacts. With increasing k^* (decreasing shear rate), the OP attains a limiting value, which asymptotically reaches its solidlike limit of 1 for significantly high values of particle-particle friction coefficient and solid volume fraction. Both Figs. 3.7(a) and 3.7(b) lead to the conclusion that the OP is able to capture the changes in particle and flow properties.

The ROP model predictions of stress are now compared to those from homogeneous shear simulations with a range of shear rates. The solid volume fraction used for the simulations ($\nu = 0.58$) was chosen to match that of the central part of the granular assembly in vertical direction from the Couette cell simulations reported earlier in this study (as noted earlier, the volume fraction field is non uniform). The particle friction coefficient μ_p and coefficient of restitution e used are the same as used in the Couette cell simulations.

Figure 3.8 shows a logarithmic plot of the elastic scaling of the shear stress as a function of shear rate. In this scaling, the stress for a quasi-static flow will appear as a horizontal line, but a line with slope of -1 in the inertial regime where the stress is proportional to $\rho d_0^3\dot{\gamma}^2$. Figure 3.8 shows that, the ROP model does not predict the correct shear stress when compared with DEM data. The slope of the data points predicted using ROP model was found to be -0.94, whereas the DEM data points follow a slope of -0.41. This difference in the magnitude and strain-rate dependence of the stress is attributed to the fact that the *fluidlike* stress is assumedly modeled by KTGF, which may not be valid in the intermediate regime where both collisional and frictional interactions between particles are important.

To further investigate the scaling of stress in the intermediate regime, we firstly decomposed the total granular stress obtained from DEM simulations into contact and

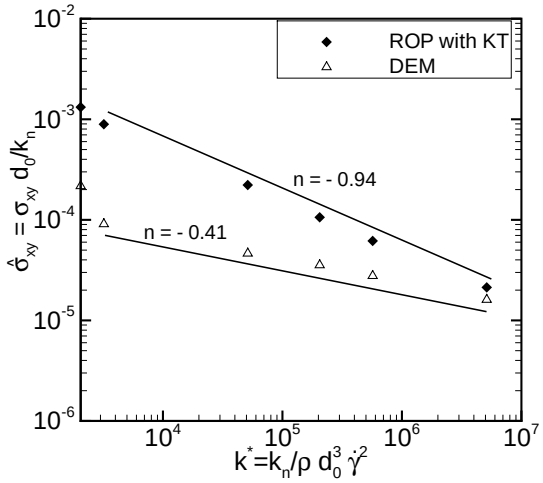

Figure 3.8 Shear stress against shear rate for homogenous shear simulations. Comparison of ROP-KT model prediction with DEM results. The open symbols corresponds to DEM data whereas the filled symbols are prediction from ROP-KT model. Simulation parameters: $\nu = 0.58$, $\mu_p = 0.19$, $e = 0.9$.

streaming contributions. In Fig. 3.9(a), the contact and streaming contributions of total shear stress are plotted against nondimensional shear rate ($k_n/\rho d_0^3 \dot{\gamma}^2$) for a similar homogeneous simulation discussed in Fig. 3.8. As expected, at this high solid volume fraction the contact part contributes more than 95% to the total granular stress. Figure 3.9(a) also shows that the contact part of the total granular stress follows the same scaling with shear rate as the total granular stress, whereas the streaming part does not exhibit this scaling.

We then decomposed the total granular stress obtained from DEM simulations into fluidlike and solidlike contributions, which are plotted in Fig. 3.9(b) against nondimensional shear rate. The contribution from the solidlike stress is about 60-70% at this nominal volume fraction and particle-particle coefficient of friction. Both the solidlike and fluidlike stress follow the same scaling ($\sigma \propto \dot{\gamma}^n, 0 < n < 2$) as the total stress

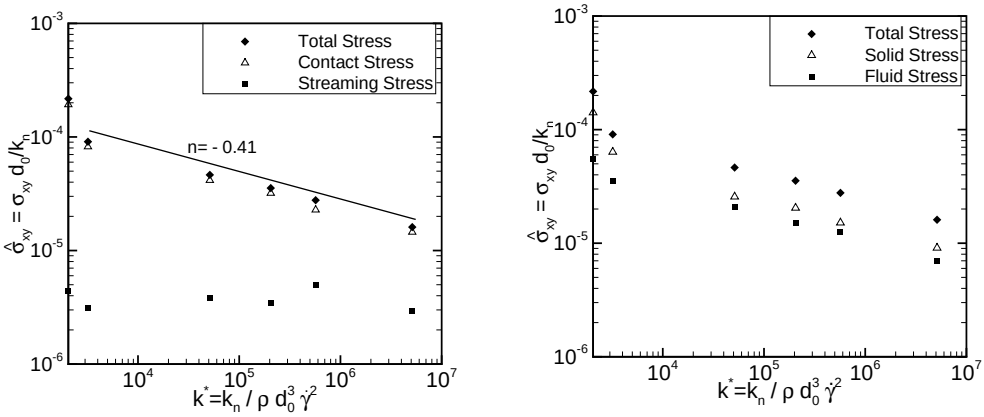

(a) (b)

Figure 3.9 (a) Decomposition of the total granular shear stress into contact (static) and streaming (dynamic) contributions. Simulation parameters: $\nu = 0.58$, $\mu_p = 0.19$, $e = 0.9$ and (b) Decomposition of the total granular shear stress into solidlike and fluidlike contributions. Simulation parameters: $\nu = 0.58$, $\mu_p = 0.19$, $e = 0.9$.

because both of them carry portions of streaming and contact stress as well–only the difference is whether the contacts are enduring or not.

3.5 Conclusions

Experimental measurements and DEM simulations have been performed for a modified annular Couette shear cell operated in batch and continuous modes with dense granular materials. Results of shear stress and the ratios to normal stress were reported. Transition from the quasi-static regime ($\sigma \neq f(\dot{\gamma})$) in the batch mode of operation to the intermediate regime ($\sigma \propto \dot{\gamma}^n, 0 < n < 2$) in the continuous mode was observed in both experiments and simulations. It has also been shown by the simulation that this transition and the power-law relation in the intermediate regime are insensitive to some particle properties, and to the vertical flow speed within a range.

A continuum model based on OP has been used to capture the intermediate behavior.

While the variation of OP itself can reflect the transitional behavior in general, the model fails to capture the correct power-law relation in the intermediate regime. A scaling analysis has revealed that in the intermediate regime the fluidlike stress has the same power-law dependence on shear rate as the total stress does, instead of the second-power dependence predicted by KTGF. This study illuminates that KTGF is not suitable as the constitutive law for the fluidlike stress in the intermediate regime and that power-law types of constitutive relations should be sought for the fluidlike (or solidlike) stress in order for the OP model to correctly predict the intermediate behavior.

CHAPTER 4. REFINED ORDER PARAMETER MODEL AND ITS PERFORMANCE IN HOMOGENEOUS SHEAR FLOWS

This chapter is a manuscript in preparation titled "Refined order parameter model and its performance in homogeneous shear flows" authored by Vidyapati, J. Sun, S. Sundaresan and S. Subramaniam.

Abstract

A linear order parameter (OP) based objective constitutive model is proposed, with new model coefficients extracted from the data of 3D DEM (discrete element method) simulations of homogeneous shear flows. This linear version of the OP model has advantage that, the total granular stress can be inverted from solidlike or fluidlike stress relations and it is denoted as the refined order parameter (ROP) model. To complete the ROP model specification, it is assumed that the fluidlike stress contribution follows the kinetic theory of granular flows (KTGF) even in the dense regime (Aranson and Tsimring, 2002). The performance of different constitutive models including the ROP model is tested by comparing its predictions for the granular stress with the DEM data. However, it is found that none of these models capture the correct scaling of shear stress with shear rate in the intermediate regime, leading to the conclusion that further development of constitutive models is needed in this regime of granular flows.

Notation for section 4.1 to section 4.6

d_0 particle diameter

dt time step for simulation

e particle restitution coefficient

F_n normal force

F_t tangential force

k^* nondimensional shear rate

k_n particle normal stiffness coefficient

m_0 particle mass

q heat flux vector

S_{ij} rate of strain tensor

T granular temperature

t time

t^* typical time of collisional for solid contacts

t_c binary collision time

U mean velocity vector

Z total number of contacts

Z_s number of solid contacts

Greek symbols

α,β,γ model coefficients for the OP model

δ_{ij} Kronecker delta

$\dot{\gamma}$ shear rate

$\hat{\epsilon}$ relative error in least–squares solution

μ_p particle friction coefficient

μ_t tangential coefficient of friction

μ_w wall friction coefficient

ν solid volume fraction

ν_{max} packed bed void fraction

ρ order parameter

ρ_s particle density

σ_0 scale of the stress

σ_{ij} total granular stress

σ_{ij}^f fluidlike contribution to the total granular stress

σ_{ij}^s solidlike contribution to the total granular stress

4.1 Introduction

A quantitative description of the large–scale behavior of the granular media requires a reliable continuum model. The difficulty in treating the granular material as a continuum is that, the grains can exhibit constitutive behavior like a solid (in sand pile), like a liquid (when poured from a hopper or silo) or like a gas (when it is strongly agitated) (Jaeger et al., 1996). These constitutive behaviors depend on the applied shear rate, solid volume fraction and interparticle friction coefficient. For the two extreme regimes (rapid and quasi–static regime), constitutive equations have been proposed based on the kinetic theory for rapid flows (Goldhirsch, 2003), and soil mechanics for slow quasi–static flow (Nedderman, 1992). However, the intermediate regime, where both collisional and frictional interactions between the particles are important, still lacks a unified theory and has motivated many studies over the past decade (Jop et al., 2006; GDR MiDi group, 2004). Nevertheless, these theories were unable to capture the transition between solidlike and fluidlike behavior of the granular material.

Savage (1998) proposed a continuum theory for slow dense granular flows based on the so–called associated flow rule that relates the strain rate and the shear stress in plastic frictional systems. Averaging strain–rate fluctuations yields a Bingham–like constitutive relation in which the shear stress has a viscous and a strain–rate independent parts. According to this theory, the stress and strain rate tensors are always coaxial and, furthermore, it also postulates that the viscosity diverges as the density approaches the close packing limit. Losert et al. (2000) proposed a similar hydrodynamic model based on a Newtonian stress–strain constitutive relation with density dependent viscosity, without a strain rate independent component. As observed in Ref. (Losert et al., 2000), the ratio of the full shear stress to the strain rate diverges at the fluidization threshold. This was also interpreted in Ref. (Losert et al., 2000) as a divergence of the viscosity coefficient when the volume fraction approaches the randomly packed limit. This description works

only in a fluidlike state and cannot properly account for hysteretic phenomena in which static and fluidized states co–exist under the same external load, such as stick–slip oscillations (Nasuno et al., 1998), avalanching (Daerr and Douady, 1999), or shear band information.

Volfson et al. (2003) proposed a different approach based on the order parameter (OP) description of the granular matter, where the total granular stress σ_{ij} is decomposed into sum of a "solidlike" σ^s_{ij} and a "fluidlike" σ^f_{ij} stress tensor, and in which the OP specifies the ratio between solid and fluid part of the stress tensor. This description based on the separation of static and fluid components of the shear stress, calls for an alternative definition of viscosity as a ratio of the fluid part of the shear stress to the strain rate, which remains finite at the fluidization threshold. Models are then proposed for the "solidlike" and "fluidlike" parts, in terms of the granular stress tensor σ_{ij}. The model proposed by Volfson et al. (2003) assumes that the principal axes of all the stress tensor are coaxial. Models for the fluidlike (or solidlike) stress tensor which requires specification of the model coefficient (that depends on ratios of individual stress tensor component) are obviously coordinate–system dependent. Therefore model such as this (Volfson et al., 2003) are not general, but are restricted to the coordinate system and flow configurations in which they are specified.

The original OP model by Volfson et al. (2003) was generalized to an objective form by Gao et al. (2005), which is coordinate system independent. However the model coefficients of the objective OP model specified by Gao et al. (2005) is based on the model coefficients that matched DEM data for 2D inhomogeneous Couette flow with wall boundary condition. In this work, the new model coefficients of the objective OP model were extracted from data of 3D DEM simulations of homogenous shear flows. A generalized version of this model (Gao et al., 2005) was further linearized which allows the inversion of the total granular stress from fluidlike or solidlike stress relations. Following Aranson and Tsimring (2002), it was assumed that the fluidlike contribu-

tion of the total granular stress can be computed from kinetic theory of granular flows (KTGF) (Lun et al., 1984). Then the performance of the ROP model is assessed by comparing its predictions for the total granular stress with DEM data in different regimes of granular flows.

4.2 Order parameter model description

The original OP model was developed by Aranson, Tsimring and Volfson in a series of papers (Volfson et al., 2003; Aranson and Tsimring, 2002). The fundamental premise of this model is that, one can define an OP in granular flows similar to that used in the Landau theory of phase transition (Landua and Lifshittz, 1980). In (Volfson et al., 2003), the OP is defined as the ratio of space–time averaged number of "enduring" contacts $\overline{\langle Z_s \rangle}$ to all contacts $\overline{\langle Z \rangle}$ within a sampling volume,

$$\rho = \frac{\overline{\langle Z_s \rangle}}{\overline{\langle Z \rangle}}. \tag{4.1}$$

The OP is useful in characterizing two limiting cases: when the granulate is in "enduring" state and when it is strongly agitated, i.e., completely fluidized. In the solid state all contacts are enduring and hence $\rho = 1$. In the fluidized case $\overline{\langle Z_s \rangle}$ is zero and $\overline{\langle Z \rangle}$ is small but finite, therefore $\rho = 0$. Since the OP distinguishes between "solidlike" contacts and "fluidlike" contacts among all contacts in the granular material, its estimation requires a precise definition of these two types of contacts. A contact is considered enduring (solidlike), if it is in stuck state ($F_t < \mu_t F_n$) and its duration is longer than a typical time of collision t^*, which is generally taken as 1.1 times the binary collision time t_c (Volfson et al., 2003). The first requirement eliminates long lasting sliding contacts, and the second requirement excludes short term collisions. When either of the requirements is not fulfilled, the contact is defined as "fluidlike".

The original OP model (Volfson et al., 2003) decomposes the total granular stress tensor into "solidlike" and "fluidlike" contributions based on the OP. The OP model

gives expression for "solidlike" and "fluidlike" stress tensors that are functions of the order parameter ρ and the total granular stress tensor σ_{ij}. The original OP model by Volfson et al. (2003) is generalized to an objective form by Gao et al. (2005). The objective expressions for σ_{ij}^f, the "fluidlike", and σ_{ij}^s, the "solidlike" contribution to the total granular stress which are co-ordinate system independent are given as follows (Gao et al., 2005),

$$\sigma_{ij}^f = \sigma_0\{\alpha\delta_{ij} + \beta b_{ij} + \gamma[(b^2)_{ij} - \frac{1}{3}(b^2)_{ll}\delta_{ij}]\}, \tag{4.2}$$

$$\sigma_{ij}^s = \sigma_0\{(1-\alpha)\delta_{ij} + (1-\beta)b_{ij} - \gamma[(b^2)_{ij} - \frac{1}{3}(b^2)_{ll}\delta_{ij}]\}, \tag{4.3}$$

where $\sigma_0 = \sigma_{ii}/3$ is the scale of stress (Einstein notation is used so summation is implied over repeated indices). The scalar model coefficients α, β, γ are functions of the invariants of the normalized, symmetric, traceless, stress anisotropy tensor b_{ij} and the order parameter ρ. The model coefficients α and β are specified by Gao et al. (2005), which were based on model coefficients that matched DEM data for 2D inhomogeneous Couette flow with wall boundary condition

$$\alpha = (1-\rho)^{1.8}, \tag{4.4}$$

$$\beta = (1-\rho)^{2.5}, \tag{4.5}$$

and b_{ij} is defined as,

$$b_{ij} = \frac{\sigma_{ij}}{\sigma_0} - \delta_{ij}. \tag{4.6}$$

The components of the second–order tensor b^2 are defined as

$$(b^2)_{ij} = b_{ik}b_{kj}, \tag{4.7}$$

and $(b^2)_{ll}$ is a scalar that is defined as

$$(b^2)_{ll} = b_{lk}b_{kl}. \tag{4.8}$$

4.3 DEM simulations of sheared granular flow

The OP is extracted by performing discrete element method (DEM) simulations of sheared granular flow on monodisperse, non–cohesive spheres of diameter d_0 and mass m_0 for a range of solid volume fractions, particle friction coefficients and shear rates. A soft sphere model is used, in which particles interact via contact laws and friction only on contact. Since the realistic modeling of particle deformation is complicated, a simplified contact force and the overlap relation (Silbert et al., 2001), the linear spring–dashpot model, is used in this work. The details of the contacts model used in the study, can be found in Silbert et al. (2001) and Sun et al. (2006).

These constant–volume DEM simulations of sheared granular flow are performed in a cubical domain of $14 \times 14 \times 14$ particle diameter units, for solid volume fraction ranging from 0.45 to 0.62. The effect of the control volume size was tested by examining cubical control volumes ranging in size from $7d_0 \times 7d_0 \times 7d_0$ to $20d_0 \times 20d_0 \times 20d_0$. No effect is found on the resultant stress as long as side of the cube selected is at least $10d_0$. A similar study was performed Campbell (2002), where he showed that the resultant stress remains unchanged as long as the dimensions were at least $7d_0 \times 7d_0 \times 7d_0$. For all the simulations reported, the mass and diameter of the particles were set to 1, so the density of the particles turns to be $6/\pi$. The value of normal spring stiffness k_n, was set to be 191000 which capture the general behavior of intermediate to high k_n system (Silbert et al., 2001). This offers a reasonable representation of realistic granular materials. The value of the coefficient of restitution e was chosen to be 0.7. All these simulations are performed with zero gravity. The homogeneous shear simulations are performed with periodic boundary conditions in all directions (x, y, z) and uniform shear is generated in the domain using the "SLLOD" algorithm (Lois et al., 2005). The time step Δt for the simulations is selected to be one fiftieth of the binary collision time t_c, which is small enough for a temporally converged numerical simulations (Silbert et al., 2001).

Simulations were run to a nondimensional time of $\dot{\gamma}t = 500$, which is long enough to attain a statically stationary solution (Campbell, 2002). After reaching the steady state, the quantities are averaged out over the number of time steps.

The OP values extracted from the 3D DEM simulations are verified by comparing them with similar calculations of Volfson et al. (2003) for 2D DEM. In Fig. 4.1 the OP is plotted as a function of solid volume fraction for an inhomogeneous wall shear simulation. The OP values are averaged across the inhomogeneous direction to obtain a single value following Volfson et al. (2003). One should note that the OP values reported by Volfson et al. (2003) were obtained from 2D DEM simulations, whereas the OP values reported in this work are extracted from 3D DEM simulations. For a meaningful comparison, the reported 2D solid volume fraction is converted to a corresponding 3D solid volume fraction by using the following relation (Wachem et al., 2001),

$$\nu_{3D} = \frac{2}{\sqrt{\pi\sqrt{3}}}\nu_{2D}^{3/2}. \tag{4.9}$$

A maximum difference of about 15% is found at solid volume fraction of 0.60. Our results verify the sudden increase in the OP as the solid volume fraction increases from 0.60 to 0.62 that is reported in Volfson et al. (2003).

As a next step, it is verified through DEM simulations of wall bounded shear flows, that the OP is indeed capable of capturing the granular phase "transition" from solidlike to fluidlike behavior. The contour plot of the OP for an inhomogeneous wall bounded shear flow is shown in Fig. 4.2. The OP takes its minimum value near the wall and its maximum value near the centerline. This near-wall behavior is justified because the granular material will behave more like a liquid near the moving walls, than near the centerline. This result shows that, the OP does captures the granular phase transition from the solidlike to fluidlike behavior.

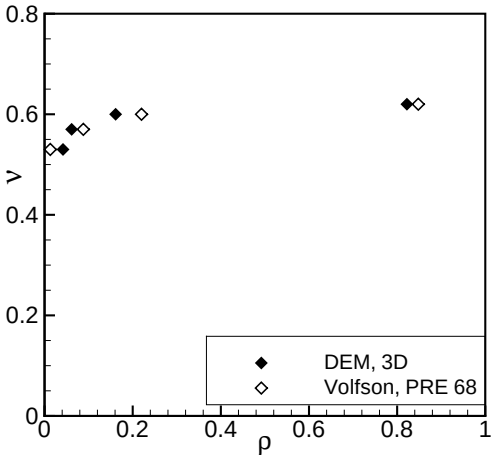

Figure 4.1 OP as a function of solid volume fraction for inhomogeneous wall shear simulation. The filled symbols represent the 3D DEM data, whereas blank symbols corresponds to Volfson et al. Volfson et al. (2003). Simulation parameters: $\mu_p = 0.5$, $\mu_w = 0.5$, $k^* = k_n/\rho_s d_0^3 \dot{\gamma}^2 = 10^5$ and $e = 0.7$.

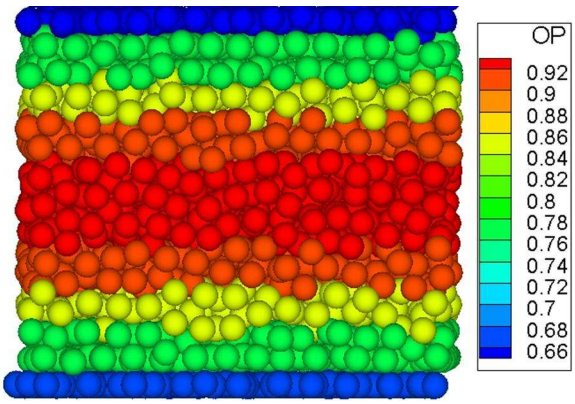

Figure 4.2 Contour plot of the OP in an inhomogeneous wall bounded shear flow, showing transition from fluidlike behavior (near the walls) to solidlike behavior (near the center of the domain). Simulation parameters: $\nu = 0.60$, $\mu_p = 0.5$, $\mu_w = 0.5$, $k^* = k_n/\rho_s d_0^3 \dot{\gamma}^2 = 10^5$ and $e = 0.7$.

4.4 Refinement of the order parameter model

The objective OP model (Gao et al., 2005), is refined by computing new model coefficients α, β and γ, that best fit the fluidlike stress tensor σ_{ij}^{f} relation given by Eq. 4.2, using data for the total granular stress σ_{ij} and fluidlike stress σ_{ij}^{f} obtained from 3D DEM simulations of homogeneous shear flow. In 3D there are six independent nonzero components of the fluidlike stress tensor (assuming the stress tensor to be symmetric). Therefore one can specify three model coefficients α, β and γ to match the six component of the "fluidlike" stress from simulations data in least–squares sense. Figure 4.3(a) shows the least–squares fit of the model coefficients α, β and γ with the OP for a nonlinear model given by Eq. 4.2. It can be inferred from Fig. 4.3(a) that, the magnitude of the third model coefficient γ remains close to zero for complete range of the OP. Note that the model coefficient γ is the coefficient multiplying only the nonlinear terms in the Eq. 4.2, this indicates possibility of forming a linear model. The model coefficients α and β corresponding to a linear objective model are computed by dropping the term containing γ in Eq. 4.2, and performing the least–squares solution from Eq. 4.10.

$$\sigma_{ij}^{f} = \sigma_0\{\alpha\delta_{ij} + \beta b_{ij}\} \tag{4.10}$$

Figure 4.3(b) shows the least–squares fit for the model coefficients α and β with the OP for the proposed linear objective model. It can be inferred from Fig. 4.3(b) that, the magnitude of the model coefficients α and β varies between 0 to 1.0. At $\rho = 0$, the model coefficients $\alpha, \beta = 1.0$, which indicates that the total granular stress is due to only fluidlike contribution at completely fluidized limit. At $\rho = 1.0$, the model coefficient $\alpha, \beta = 0.0$, which indicates that the total granular stress is due to only solidlike contribution. The error incurred in both (nonlinear and linear) objective model is quantified by the vector norm of the relative error in the least–squares solution, which

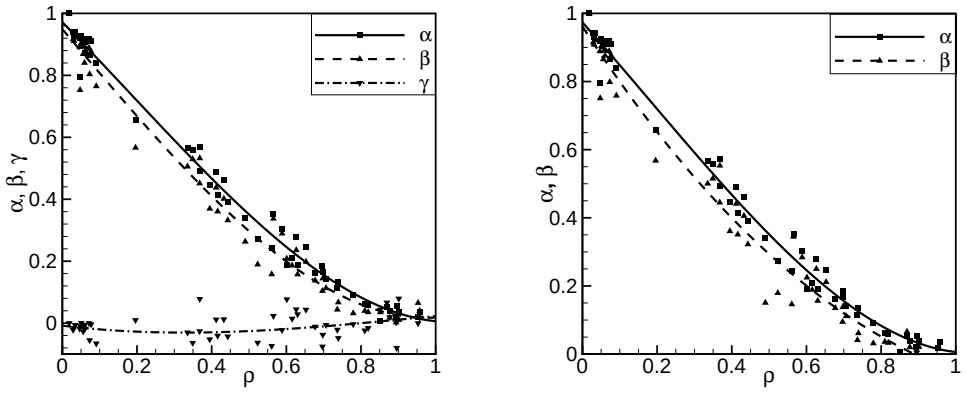

(a) (b)

Figure 4.3 (a) The OP objective model coefficients as a function of the order parameter for a nonlinear objective model, and (b) The OP objective model coefficients as a function of the order parameter for a linear objective model.

is given by Eq. 4.11.

$$\hat{\epsilon} = \frac{||\mathbf{Kx} - \mathbf{y}||_2}{||\mathbf{y}||_2} \tag{4.11}$$

In Eq. 4.11, $\mathbf{x}$ is the solution vector for the model coefficients, $\mathbf{Kx}$ is the total granular stress components given by the OP model and $\mathbf{y}$ is the total granular stress from DEM. The error incurred in terms of vector norm is depicted in the Fig. 4.4 for complete range of the OP for both nonlinear and linear objective models. As Fig. 4.4 shows, that the error incurred in both the objective models is less than 11%. The percentage error incurred in the linear model is approximately same as the error incurred in the nonlinear model, which indicates possibility of simplifying the objective OP model without losing its accuracy. Therefore, a linear version of the objective OP model with new model coefficient extracted from 3D DEM data of homogeneous shear flow is proposed. This linear version of the objective OP model is referred as refined order parameter model (ROP). The model equations for ROP model is given as follows,

$$\sigma_{ij}^f = \sigma_0\{\alpha\delta_{ij} + \beta b_{ij}\}, \tag{4.12}$$

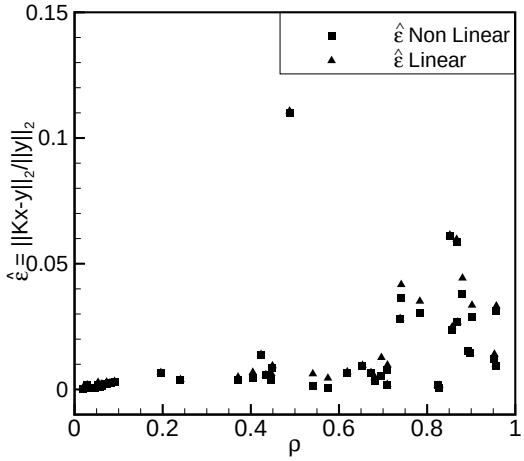

Figure 4.4 Error in the total granular stress objective models as a function of the OP for both linear and nonlinear models.

$$\sigma_{ij}^{s} = \sigma_0\{(1-\alpha)\delta_{ij} + (1-\beta)b_{ij}\}. \tag{4.13}$$

The first model coefficient α, of the linear ROP model is specified as

$$\alpha = a + b\rho + c\rho^2 + d\rho^3, \tag{4.14}$$

with $a = 0.97$, $b = -1.23$, $c = -0.31$ and $d = 0.57$. The second model coefficient β, is given as

$$\beta = A + B\rho + C\rho^2 + D\rho^3, \tag{4.15}$$

with $A = -0.96$, $B = -1.69$, $C = 0.75$ and $D = -0.07$. The advantage of the proposed linear ROP model is that, now the total granular stress can be inverted from the solidlike and fluidlike stress relations. To complete the constitutive model specification of the ROP model, it is assumed that the contributions from "fluidlike" stress agrees well with the kinetic theory of granular flows (KTGF) even in the dense regime (Aranson and Tsimring, 2002). The kinetic theory closures are taken from Lun et al. (1984) as given in Srivastava and Sundaresan (2003) to compute the fluidlike contribution of the total granular stress tensor.

Once the fluidlike contribution of the total granular stress is known, the total granular stress tensor can be expressed in terms of the "fluidlike" stress and the ROP model coefficients (α and β). The following sets of equations provide the closure for the fluidlike contribution of the total granular stress tensor,

$$\sigma_{ij}^{f} = \left[\rho_s \nu \left(1 + 4\eta\nu g_0\right) T - \eta\mu_b \nabla \cdot \mathbf{U}\right] \delta_{ij} - \left(\frac{2+\alpha}{3}\right) \times \left\{ \frac{2\mu}{g_0 \eta \left(2-\eta\right)} \left(1 + \frac{8}{5}\nu\eta g_0\right) \left[1 + \frac{8}{5}\eta\left(3\eta - 2\right) g_0\right] + \frac{6}{5}\eta\mu_b \right\} S_{ij}, \tag{4.16}$$

$$S_{ij} = \frac{1}{2}\left(\frac{\partial U_i}{\partial x_j} + \frac{\partial U_j}{\partial x_i}\right) - \frac{1}{3}\frac{\partial U_i}{\partial x_i}, \tag{4.17}$$

$$\mu = \frac{5\rho_s d(\pi T)^2}{96}, \tag{4.18}$$

$$\mu_b = \frac{256\mu\nu^2 g_0}{5\pi}, \tag{4.19}$$

$$\eta = \frac{(1+e)}{2}, \tag{4.20}$$

$$g_0\left(\nu\right) = \frac{1}{1 - \left(\nu/\nu_{max}\right)^{1/3}}, \tag{4.21}$$

$$\alpha = 1.3, \tag{4.22}$$

where σ_{ij}^{f} is the fluidlike part of the stress tensor, ρ_s is the density of the solid particle, ν is the solid volume fraction, T is the granular temperature, $\mathbf{U}$ is the mean velocity vector, S_{ij} is the strain rate tensor.

The ROP model with kinetic theory assumption for the fluidlike stress needs knowledge of the granular temperature (see Eq. 4.16). To this end we solved the pseudo–thermal energy equation (Eq. 4.23) using Euler's explicit method.

$$\frac{3}{2}\rho_s \nu \left[\frac{\partial T}{\partial t} + \mathbf{u} \cdot \nabla T\right] = -\nabla \cdot \mathbf{q} - \sigma^{f} : \nabla \mathbf{u} - J_{coll} - J_{vis} \tag{4.23}$$

The first term on the right-hand side of the above equation represents the diffusive transport of PTE (pseudo–thermal energy), where $\mathbf{q}$ is the PTE flux vector. The second term represents the rate of production of PTE by shear. The third term in Eq. 4.23 represents

the dissipation of PTE through inelastic collisions, whereas fourth term denotes the net dissipation of PTE through fluid particle interactions which is zero if only solid particles are present. The closure relation for $\mathbf{q}$ and J_{coll} is modeled following Lun et al. (1984),

$$\mathbf{q} = -\frac{\lambda}{g_0}\left(\left\{1+\frac{12}{5}\nu\eta g_0\right)\left[1+\frac{12}{5}\eta^2\left(4\eta-3\right)\nu g_0\right] + \frac{64}{25\pi}\left(41\eta-33\right)\left(\eta\nu g_0\right)^2\right\}\nabla T, \tag{4.24}$$

$$J_{coll} = \frac{48}{\sqrt{\pi}}\eta\left(1-\eta\right)\frac{\rho_s\nu^2}{d_0}g_0T^{3/2}, \tag{4.25}$$

where the parameter λ is given as following,

$$\lambda = \frac{75\rho_s d_0(\pi T)^{1/2}}{48\eta\left(41-33\eta\right)}. \tag{4.26}$$

For a homogeneously sheared granular flow (in absence of fluid phase) the PTE equation (Eq. 4.23) takes the following form,

$$\frac{3}{2}\rho_s\nu\frac{\partial T}{\partial t} = -\sigma^f : \nabla\mathbf{u} - J_{coll}. \tag{4.27}$$

The initial guess for the solution is provided using algebraic equation for granular temperature, which is derived by equating production to the dissipation (MFIX, 1993),

$$T = \left\{\frac{-K_1\nu S_{ii} + \sqrt{{K_1}^2(S_{ii})^2\nu^2 + 4K_4\nu\left[K_2(S_{ii})^2 + 2K_3\left(S_{ij}S_{ij}\right)\right]}}{2\nu K_4}\right\}^2, \tag{4.28}$$

where constants K_1, K_2, K_3 and K_4 are given as follows,

$$K_1 = 2\left(1+e\right)\rho_s g_0, \tag{4.29}$$

$$K_2 = 4d_0\rho_s\left(1+e\right)\nu g_0/\left(3\sqrt{\pi}\right) - \frac{2}{3}K_3, \tag{4.30}$$

$$K_3 = \frac{d_0\rho_s}{2}\left[\frac{\sqrt{\pi}}{3\left(3-e\right)}\left[0.5\left(3e+1\right) + 0.4\left(1+e\right)\left(3e-1\right)\nu g_0\right] + \frac{8\nu g_0\left(1+e\right)}{5\sqrt{\pi}}\right], \tag{4.31}$$

$$K_4 = \frac{12\,(1-e^2)\,\rho_s g_0}{d_0\sqrt{\pi}}. \tag{4.32}$$

The accuracy of this method is verified by comparing the granular temperature obtained by solving PTE equation with that obtained from the DEM simulations. Table 4.1 shows this comparison for range of solid volume fractions. The interparticle friction coefficient used for these simulations is 0.5, with a coefficient of restitution of 0.7. The nondimensional shear rate $k^* = k_n/\rho_s d_0^3\dot{\gamma}^2$ is set to be 10^5. It can be inferred from Table 4.1 that, the maximum difference in the granular temperature obtained from PTE solution and DEM simulation is about 15%.

Table 4.1 Comparison of granular temperature $\hat{T} = T/(d_0\dot{\gamma})^2$ obtained from PTE solution and DEM. Simulation parameters: $\mu_p = 0.5$, $e = 0.7$ and $k^* = k_n/\rho_s d_0^3\dot{\gamma}^2 = 10^5$.

Solid volume fraction	PTE solution	DEM
0.45	0.529	0.603
0.53	0.514	0.570
0.58	0.508	0.553
0.60	0.505	0.550
0.62	0.503	0.528

To compute the model coefficients α and β, knowledge of the OP is required (see Eqs. 4.14 and 4.15). To this end we curve fit the data for the OP obtained from 3D DEM simulations of homogeneous shear flows with solid volume fraction for a set of shear rates and particle friction coefficients. In Fig. 4.5(a) the OP is plotted with solid volume fraction for a nondimensional shear rate $k^* = k_n/\rho_s d_0^3\dot{\gamma}^2$ of 2.5×10^4, for a homogeneous shear simulation. It can be inferred from Fig. 4.5(a) that the OP is indeed a strong function of the particle friction coefficient. An increase of about 300% in the value of the OP is seen when particle–particle coefficient of friction increases from 0.1 to 1.0. This is expected because the number of "solid" contacts increases with increase in the interparticle friction coefficient. Effect of solid volume fraction on the OP is seen

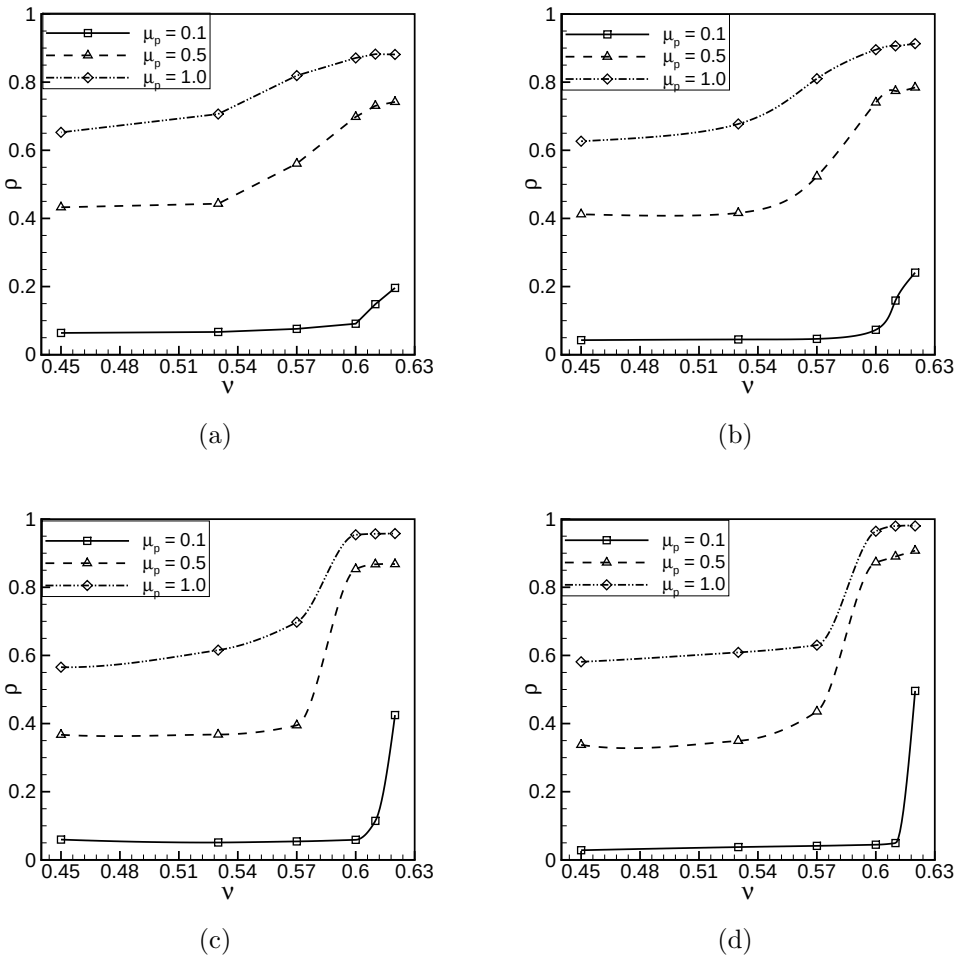

Figure 4.5 (a) The OP plotted with solid volume fraction for $k^* = 2.5 \times 10^4$ and $e = 0.7$, (b) The OP plotted with solid volume fraction for $k^* = 10^5$ and $e = 0.7$, (c) The OP plotted with solid volume fraction for $k^* = 10^7$ and $e = 0.7$ and (d) The OP plotted with solid volume fraction for $k^* = 10^9$ and $e = 0.7$.

only in the dense regime (once the solid volume fraction exceeds 0.57). A sudden jump in the value of the OP is seen near the maximum packing limit, this sudden increase in the value of the OP is ascribe to the presence of strong force chains near the maximum packing limit. Figures 4.5(b), 4.5(c), and 4.5(d) are the similar plots of the OP with solid volume fraction as described in Fig. 4.5(a), but for different values of shear rates. Looking in to these plots (Figs. 4.5(a), 4.5(b), 4.5(c), 4.5(d)) one can infer that the shear rate has the least impact on the OP, when compared to solid volume fraction and particle friction coefficient.

With the specification of the fluidlike contribution to the total granular stress σ_{ij}^{f} and the model coefficients one can solve for the total granular stress σ_{ij} using the ROP model. Equation 4.12 can be inverted to get the total granular stress for a homogeneously sheared granular assembly. Figure 4.6 depicts a flow chart for calculation of the total granular stress using the ROP model for a homogenously sheared granular assembly.

4.5 Assessment of the ROP model for homogeneous shear flows

The ROP (refined order parameter) model predictive capability is assessed by comparing its predictions to those from DEM simulations of homogeneous shear flows. The validity of kinetic theory is also assessed by comparing the contribution of the fluidlike stress tensor σ_{ij}^{f} obtained from the kinetic theory (Lun et al., 1984) with the corresponding fluidlike stress tensor obtained from the DEM data.

Figure 4.7(a) shows a logarithmic plot of the elastic scaling of the shear stress as a function of shear rate. In this scaling, the stress for a quasi–static flow will appear as a horizontal line, but a line with the slope of -1 in the inertial regime where the stress is proportional to $\rho_s d_0^3 \dot{\gamma}^2$. Figure 4.7(a) shows the variation of fluidlike stress tensor with shear rate for a solid volume fraction of 0.45. The fluidlike contribution

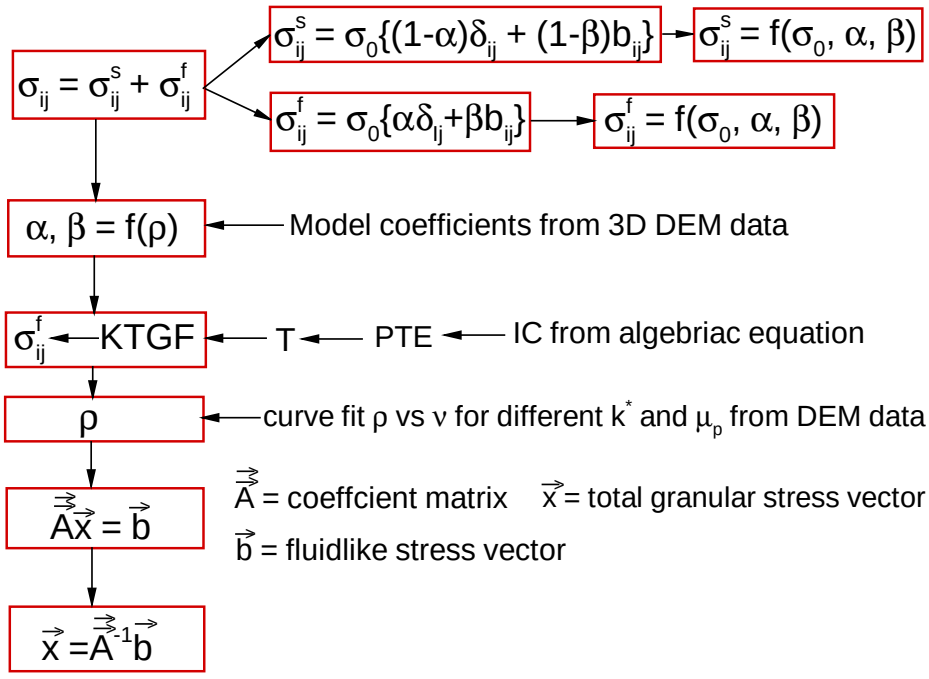

Figure 4.6 Flow chart for computation of the total granular stress using ROP model applied to homogenous shear flows.

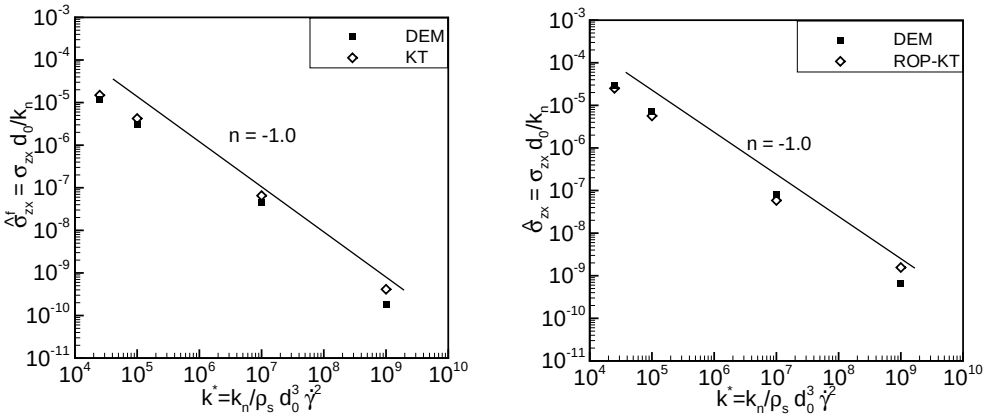

(a) (b)

Figure 4.7 (a) The fluidlike stress contribution to the total granular stress as a function of shear rate k^*. Simulation parameters: $\nu = 0.45$, $\mu_p = 0.5$, $e = 0.7$ and (b) The total granular stress as a function of shear rate k^*. Simulation parameters: $\nu = 0.45$, $\mu_p = 0.5$, $e = 0.7$.

obtained from the kinetic theory is shown by blank diamonds, whereas the filled squares shows the data directly obtained from the DEM simulations of homogeneously sheared granular flow. It can be inferred from Fig. 4.7(a) that, the fluidlike contribution to the total granular stress obtained using kinetic theory closely follows the fluidlike stress contribution obtained from the DEM simulations. Both the DEM data and predictions obtained from kinetic theory follows the inertial scaling of the stress ($\sigma \propto \dot{\gamma}^2$) with the shear rate. In Fig. 4.7(b) the shear component of the total granular stress is plotted with shear rate k^* for a nominal volume fraction of 0.45. It is clear from Fig. 4.7(b) that, the total granular stress predicted using ROP model coupled with kinetic theory (fluidlike contribution of the total granular stress obtained from the kinetic theory) closely follows the data obtained from the DEM simulations. The ROP model is able to predict the total granular stress within accuracy of 5% with the data from the DEM simulations in the inertial regime. The total granular stress obtained from both the studies follows the inertial scaling of the stress ($\sigma \propto \dot{\gamma}^2$) with the applied shear rate, this type of scaling

of the shear stress with the applied shear rate has been previously noticed by Campbell (2002) in the inertial regime of the granular flows.

In order to quantify the performance of the ROP model near the transition from inertial to intermediate regime, the assessment of the ROP model is performed for a solid volume fraction of 0.57. In Fig. 4.8(a) the variation of the fluidlike contribution of the stress (obtained from kinetic theory as well as from the DEM data) is shown with the shear rate. This plot shows, that the kinetic theory perform reasonably well in predicting the fluidlike stress contribution when compared with the data obtained from the DEM simulations in this regime. The fluidlike contribution to the total granular stress obtained from the kinetic theory follows the inertial scaling of the stress, whereas the data obtained from the DEM simulations start to deviate from the inertial scaling and shows the power law behavior of stress ($\sigma \propto \dot{\gamma}^n, 0 < n < 2$) with shear rate. Figure 4.8(b) is a similar plot as Fig. 4.8(a) but this plot compares the prediction of the ROP model for the total granular stress with data from the DEM simulations. It can been seen from Fig. 4.8(b) that at this solid volume fraction also the predictions from the ROP model when coupled to the kinetic theory is able to predict the total granular stress reasonably well. However, the predictions for the total granular stress obtained by ROP model coupled with the kinetic theory under predicts the total granular stress by about 15% when compared to the DEM data.

To assess the performance of the ROP model in the intermediate regime, simulation with solid volume fraction of 0.62 with a interparticle friction coefficient of 0.1 is selected. Figure 4.9(a) shows the variation of the fluidlike contribution of the total granular stress obtained from kinetic theory with its value obtained from the DEM simulations. It can be seen from the Fig. 4.9(a) that the kinetic theory fails to predict the correct fluidlike stress contribution in the intermediate regime when compared with data from DEM simulations. The fluidlike contribution obtained from DEM data clearly shows the intermediate scaling of the stress ($\sigma \propto \dot{\gamma}^n, 0 < n < 2$) with shear rate, whereas the

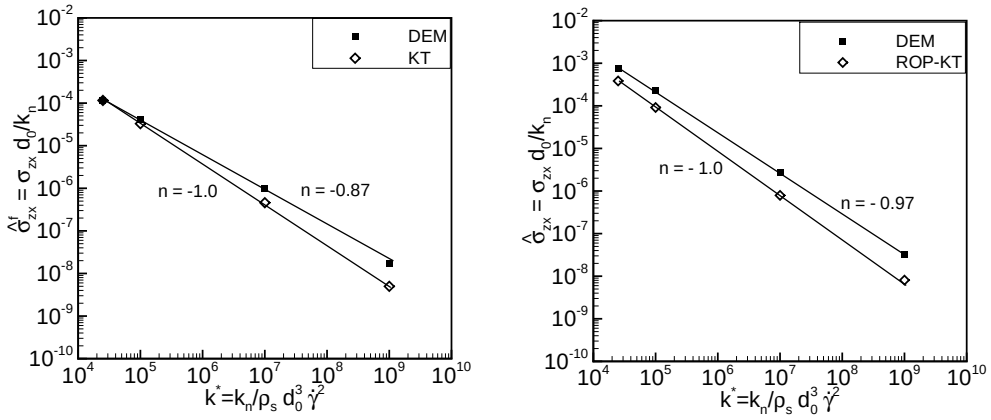

(a) (b)

Figure 4.8 (a) The fluidlike stress contribution to the total granular stress as a function of shear rate k^*. Simulation parameters: $\nu = 0.57$, $\mu_p = 0.5$, $e = 0.7$ and (b) The total granular stress as a function of shear rate k^*. Simulation parameters: $\nu = 0.57$, $\mu_p = 0.5$, $e = 0.7$.

predictions based on kinetic theory still follows the inertial scaling of the stress ($\sigma \propto \dot{\gamma}^2$) with applied shear rate. In Fig. 4.9(b) the variation of the total granular stress is plotted with the shear rate for its value obtained from ROP model and data obtained from the DEM simulations. Figure 4.9(b) shows that in the intermediate regime there are significant differences between the predictions of the ROP model with the DEM data for the total granular stress. The total granular stress obtained from the DEM data clearly shows the intermediate scaling of the stress ($\sigma \propto \dot{\gamma}^n, 0 < n < 2$) with shear rate, whereas the predictions from ROP model still follows the inertial scaling of the stress ($\sigma \propto \dot{\gamma}^2$) with shear rate.

Based on this assessment study, it can be concluded that the ROP model (coupled with the kinetic theory for the fluidlike contribution of the total granular stress) has capability to predict accurate granular stress till the solid volume fraction of 0.57. As the nominal volume fraction exceeds beyond 0.57 the flow transition takes place from inertial to intermediate regime and the ROP model coupled with the kinetic theory

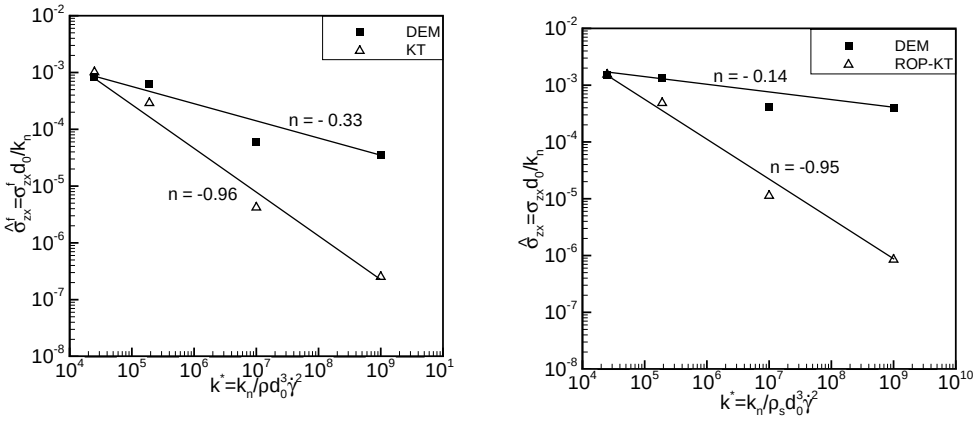

(a) (b)

Figure 4.9 (a) Fluidlike stress contribution to the total granular stress as a function of shear rate. Simulation parameters: $\nu = 0.62$, $\mu_p = 0.1$, $e = 0.7$ and (b) The total granular stress as a function of shear rate. Simulation parameters: $\nu = 0.62$, $\mu_p = 0.1$, $e = 0.7$.

fails to capture the correct trends of shear stress with shear rate. The differences in the magnitude of the stress prediction in the intermediate regime is attributed to the fact that, the ROP model coupled with the kinetic theory assumes that the fluidlike stress contribution follows the kinetic theory even in the dense regime. However this assumption does not hold in the intermediate regime where both collision and frictional interactions between the particles are important.

To further investigate the scaling of the stress in the intermediate regime, the total granular stress obtained from the DEM simulations of homogeneously sheared granular flow is decomposed into contact (virial) and streaming (dynamic) contributions. In Fig. 4.10(a) the contact contribution of the total granular stress is plotted with shear rate for a range of solid volume fractions. Figure 4.10(a) shows that the contact contribution of the total granular follows the same scaling ($\sigma \propto \dot{\gamma}^n, 0 < n < 2$) with shear rate as the total granular stress in the intermediate regime (data points correspond to the intermediate regime are shown with blank squares). However, the streaming contribution

of the total granular stress in the intermediate regime still follows the inertial scaling of the stress ($\sigma \propto \dot{\gamma}^2$) with the shear rate. As expected, at this high solid volume fraction the contact part contributes more than 95% to the total granular stress.

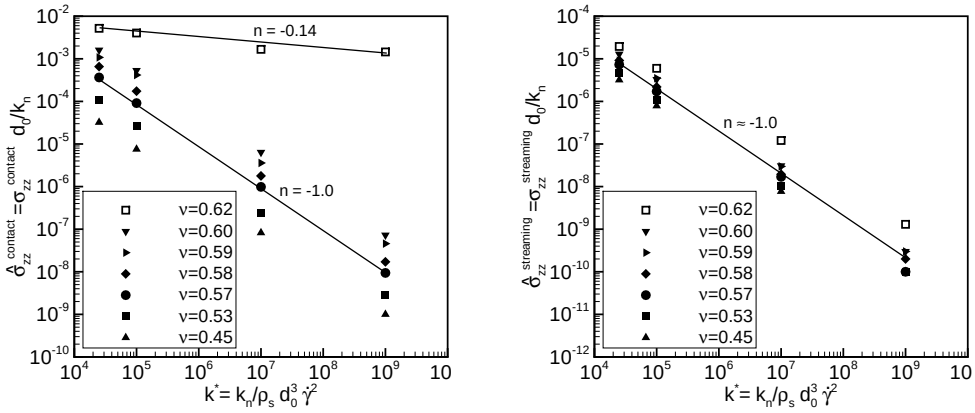

(a) (b)

Figure 4.10 (a) Contact (virial) contribution of the total granular stress as a function of shear rate. Simulation parameters: $\mu_p = 0.1$, $e = 0.7$ and (b) Streaming (dynamic) contribution of the total granular stress as a function of shear rate. Simulation parameters: $\mu_p = 0.1$, $e = 0.7$. The data points correspond to the intermediate regime is shown with blank square symbols.

Furthermore, the total granular stress obtained from the DEM simulations is decomposed into solidlike and fluidlike contributions (based on the OP model). These contributions to the total granular stress are plotted with shear rate k^*, in Figs. 4.11(a) and 4.11(b). It is interesting to observe that both the solidlike and fluidlike stress follow the same scaling ($\sigma \propto \dot{\gamma}^n, 0 < n < 2$) as the total granular stress because both of them carry portions of streaming and contact stress as well; only the difference is whether the contacts are enduring or not.

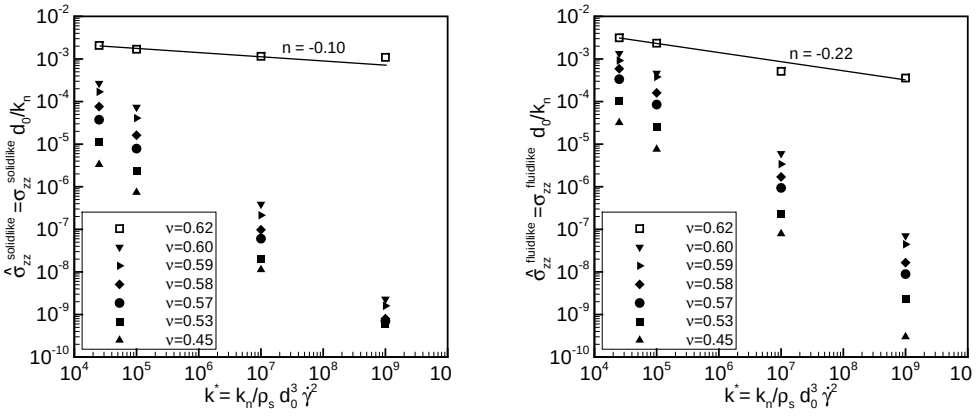

(a) (b)

Figure 4.11 (a) Solidlike contribution of the total granular stress as a function of shear rate. Simulation parameters: $\mu_p = 0.1$, $e = 0.7$ and (b) Fluidlike contribution of the total granular stress as a function of shear rate. Simulation parameters: $\mu_p = 0.1$, $e = 0.7$. The data point correspond to the intermediate regime is shown with blank square symbols.

4.5.1 Performance evaluation of different constitutive models in intermediate regime

The performance of different constitutive models is assessed in the intermediate regime of granular flows. In Fig. 4.12, shear component of the total granular stress is plotted with shear rate for a solid volume fraction of 0.62 with interparticle friction coefficient of 0.1. The different constitutive models assessed are listed below:

1. ROP–KT: This is the constitutive model proposed in present work, where the ROP model is linked with the kinetic theory of granular flows (KTGF) (Lun et al., 1984) for the fluidlike stress contribution of the total granular stress. As discussed earlier, this model fails to capture the correct trends of shear stress with shear rate in the intermediate regime.

2. ROP–DEM: In this constitutive model, the fluidlike (or solidlike) contribution to

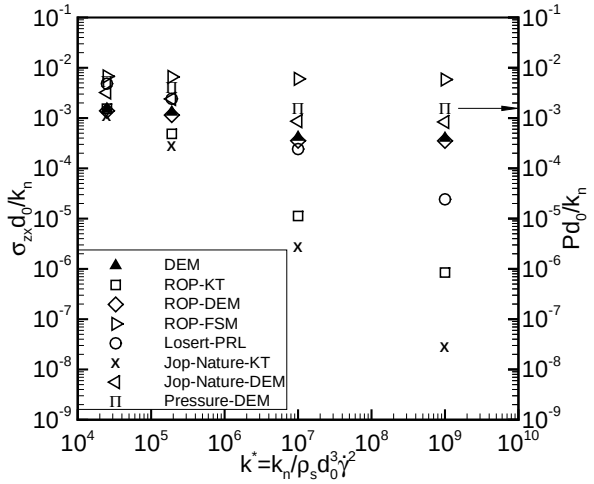

Figure 4.12 Shear component of the total granular stress (different symbols represent result obtained with different constitutive models) plotted with shear rate. Simulation parameters: $\nu = 0.62$, $\mu_p = 0.1$, $e = 0.7$.

the total granular stress is supplied form the DEM data and then the ROP model is solved to compute the total granular stress. Figure 4.12 shows that, the ROP–DEM model is capable of predicting the total granular stress accurately (within 10%) even in the intermediate regime, provided that the fluidlike (or the solidlike) stress contribution is taken from the DEM data. Hence, the limitation is **not** in the objective ROP model concept, but in the constitutive model for the fluidlike (or solidlike) stress contributions in the intermediate regime.

3. ROP–FSM: The FSM (frictional stress model) is proposed by Srivastava and Sundaresan (2003) for the frictional part of the total granular stress. The FSM model is used to compute the solidlike stress contribution, then the ROP model is solved to obtain the total granular stress. This frictional stress model is based on the critical state theory of soil mechanics. With the critical state assumption, where the granular assembly deforms without any volume change, the frictional contribution

of the stress is give by,

$$\frac{\sigma^{fric}}{p_c(\nu)} = \mathbf{I} - \sqrt{2}\sin\phi\frac{\mathbf{S}}{\sqrt{\mathbf{S}:\mathbf{S}}}, \tag{4.33}$$

where form of $p_c(\nu)$ (critical state pressure) is taken from Johnson and Jackson (1987)

$$p_c(\nu) = \begin{cases} F\frac{(\nu-\nu_{min})^r}{(\nu_{max}-\nu)^s} & \text{if } \nu > \nu_{min} \\ 0 & \text{if } \nu \leq \nu_{min} \end{cases} \tag{4.34}$$

where F, r and s are constants, taken from Srivastava and Sundaresan (2003). As shown in Fig. 4.12 this model when linked with the ROP model for the solidlike stress contribution, predicts stresses which are independent of the shear rate (a behavior similar to quasi–static regime). However, the data obtained from the DEM simulations show a dependency of shear stress on the shear rate in this regime.

4. Losert–PRL: Losert et al. (2000) proposed a constitutive model with density dependent viscosity. The shear stress in this model is given as,

$$\sigma_{xy} = \eta\dot{\gamma} \tag{4.35}$$

where viscosity is related with the density as follows,

$$\eta = (\nu_{max} - \nu)^{-1.75}. \tag{4.36}$$

Figure 4.12 shows that, the shear stress predicted using this model fails to capture the correct scaling of shear stress with shear rate in the intermediate regime.

5. Jop–Nature: Jop et al. (2006) described the granular material as an incompressible fluid with the internal stress tensor given by the following relations,

$$\sigma_{ij} = -P\delta_{ij} + \tau_{ij} \tag{4.37}$$

$$\tau_{ij} = \eta\left(|\dot{\gamma}|, P\right)\dot{\gamma}_{ij} \tag{4.38}$$

with, $\eta\left(|\dot{\gamma}|, P\right) = \mu\left(I\right)P/|\dot{\gamma}|$ and $I = |\dot{\gamma}|d/\left(P\rho_s\right)^{0.5}$, where $\dot{\gamma}_{ij} = \partial u_i/\partial x_j + \partial u_j/\partial x_i$ is the strain rate tensor and $|\dot{\gamma}| = \left(0.5\dot{\gamma}_{ij}\dot{\gamma}_{ij}\right)^{0.5}$ is the second invariant of $\dot{\gamma}_{ij}$. In this rheology, P represents an isotropic pressure, and $\eta\left(|\dot{\gamma}|, P\right)$ is an effective viscosity, which definition is related to the friction coefficient $\mu\left(I\right)$ as follows,

$$\mu(I) = \mu_s + (\mu_2 - \mu_s)/(I_0/I + 1). \tag{4.39}$$

However, the closure for the isotropic pressure P is not specified in this work. The closure equation for the P is provided from kinetic theory (Lun et al., 1984) and then the total granular stress is obtained using this model. As shown in Fig. 4.12 this model coupled with the kinetic theory (Jop–Nature–KT) for the isotropic pressure fails to capture the correct trends of shear stress with shear rate in the intermediate regime. However, when the isotropic pressure P is supplied from the DEM data (Jop–Nature–DEM) the model captures the correct trend of shear stress with the shear rate in the intermediate regime.

Figure 4.12 also shows the variation of the isotropic pressure (right Y axis) obtained from the DEM simulations with shear rate for a homogeneously sheared granular assembly. It can be inferred from this plot that the pressure follows the same scaling with shear rate as the shear stress in the intermediate regime. Hence it is very important for a continuum model to predict the correct behavior of the pressure with strain rate.

4.6 Conclusions

A linear objective OP based continuum model with new model coefficients extracted from the data of 3D DEM simulations of homogeneous shear flow is proposed. The advantage of this linear objective OP model (ROP model) is that now the total granular stress can be inverted from the solidlike and fluidlike stress relations. The error incurred

in the prediction of the total granular stress is quantified for both the nonlinear and linear models, and shown to be below 11% for complete range of the OP. To complete the ROP model specification, it is assumed that the fluidlike contribution follows the kinetic theory of the granular flows (KTGF) even in the dense regime (Aranson and Tsimring, 2002). The performance of the ROP model is assessed by comparing its prediction for the total granular stress with the 3D DEM data of homogenously sheared granular flows. This study reveals that the ROP model has capability to predict the accurate (within accuracy of 15%) granular stress up to a solid volume fraction of 0.57. As the solid volume fraction increases beyond 0.57, the flow transition from inertial to intermediate regime takes place and the ROP model coupled with the kinetic theory (for fluidlike stress contribution) fails to capture the correct trends of the shear stress with shear rate. This discrepancy in prediction of the total granular stress is attributed to the fact that, the ROP model coupled with kinetic theory assumes that the fluidlike contribution to the total granular stress can be computed from the kinetic theory even in the dense regime. However, this assumption works only in the inertial (rapid flow) regime of the granular flows, where only binary interactions are considered. In the intermediate regime, both the collisional and frictional interactions between the particles are important and kinetic theory fails to capture this behavior.

The assessment study performed with different constitutive models in the intermediate regime, reveals that none of these existing models captures the correct scaling of shear stress with shear rate in this regime. However, the ROP and the model proposed by Jop et al. (2006) captures the correct scaling of shear stress with shear rate, provided one of the inputs to the model is supplied from the DEM data. This result also indicates that, the ROP model is capable enough of predicting the accurate total granular stress in the intermediate regime, provided its inputs (solidlike or fluidlike stress contributions) are correct. Hence it will be a future work to seek more accurate models for these contributions (fluidlike or solidlike stress) to the total granular stress, which can be coupled

with the ROP model to predict the accurate total granular stress in the intermediate regime.

CHAPTER 5. CONCLUSIONS AND FUTURE WORK

5.1 Conclusions

In this study DEM simulations and constitutive models have been used to understand the rheological behavior of dense granular flow, in particular, the regime transition phenomenon from quasi–static to rapid flow regime. The specific accomplishments of this study are as follows:

1. DEM simulations were performed with an existing code LAMMPS (Plimpton, 1995) that was modified to extract quantities such as order parameter (OP), solid-like and fluidlike contributions of the total granular stress.

2. A computational setup was devised to simulate gravity–driven sheared granular flow between planar walls that mimics Couette–cell experiments performed by Langroudi et al. (2010).

3. An OP (order parameter) based constitutive model was refined and a linear model (ROP model) with new model coefficients was proposed.

4. Performance of different constitutive models in the intermediate regime of granular flows was evaluated.

In chapter 3, the rheology of dense granular material in an annular Couette cell is modeled using DEM, and compared with experiments performed by Langroudi et al. (2010). A transition from the quasi–static ($\sigma \neq f(\dot{\gamma})$) in the batch mode of operation

to the intermediate regime ($\sigma \propto \dot{\gamma}^n, 0 < n < 2$) in the continuous mode was observed in both experiments and DEM simulations. It has also been shown by the simulations that this transition and the power–law relation in the intermediate regime are insensitive to some particle properties, and to the vertical flow speed within the range. A continuum model based on the OP (order parameter) has been used to capture the intermediate behavior. While the variation of OP reflects the transitional behavior in general, the model fails to capture the correct power–law relation in the intermediate regime. This study also reveals that KTGF is not suitable to describe the rheological behavior for the fluidlike stress in the intermediate regime, and the power–law types of constitutive relations should be sought for the fluidlike (or the solidlike) stress.

In chapter 4, a linear objective OP–based continuum model with new model coefficients extracted from the data of 3D DEM simulations of homogeneous shear flow is proposed. This ROP model has the advantage that the total granular stress can be inverted from solidlike and fluidlike stress relations. To complete the ROP model specification it is assumed that the fluidlike contribution follows the kinetic theory of granular flows (KTGF) even in the dense regime. The performance of the ROP model is assessed by comparing its predictions with DEM data in different regimes of the granular flows. This study reveals that the ROP model has capability to accurately predict the granular stress to within 15% error, up to a solid volume fraction of 0.57. As the solid volume fraction increases beyond 0.57 the flow transition from inertial to intermediate regime takes place and the ROP model coupled with kinetic theory (for fluidlike stress contribution) fails to capture the correct trend of shear stress against shear rate. This discrepancy in the prediction of the total granular stress is attributed to the fact that, the ROP model coupled with the kinetic theory assumes that the fluidlike contribution to the total granular stress can be computed from the kinetic theory even in the dense regime. Other constitutive models were also evaluated in the same intermediate regime and it was found that none of these models capture the correct scaling of shear stress

with shear rate in this regime.

In summary, DEM is a useful approach to understand the behavior of granular flow, and to develop and assess constitutive models. DEM's qualitative predictions and detailed information about the granular microstructure make it a valuable tool to develop constitutive models. Although the OP concept is a promising approach to capture the granular phase transition, the assumption that the fluidlike stress can be modeled using kinetic theory of granular flows does not hold in the intermediate regime where both collisional and frictional (enduring) contacts between the particles are important.

5.2 Future work

Results of this study show that the constitutive modeling of the intermediate regime behavior of granular flow is the biggest challenge. It will require a constitutive model that can capture the correct power–law behavior of the stress with the strain rate. The OP seems to be a promising concept because it can capture the granular phase transition from solidlike to fluidlike behavior. However, there is considerable scope for improvement before it can be used as a predictive model in the intermediate regime. One of the important results of this study indicate that the ROP model is capable enough of predicting the accurate total granular stress in the intermediate regime, provided its inputs (solidlike or fluidlike stress contributions) are correct. Hence there is need for an accurate stress model based on microscale physics in the intermediate regime that can be used in the ROP framework to predict the correct total granular stress.

APPENDIX A. CONTACT MODEL DESCRIPTION

For two contacting particle $\{i,j\}$, with radii $\{a_i,a_j\}$ at positions $\{\mathbf{r}_i,\mathbf{r}_j\}$, with velocities $\{\mathbf{v}_i,\mathbf{v}_j\}$ and angular velocities $\{\boldsymbol{\omega}_i, \boldsymbol{\omega}_j\}$, the normal compression δ_{ij}, relative normal velocity $\mathbf{v}_{n_{ij}}$, and relative tangential velocity $\mathbf{v}_{t_{ij}}$ are (Silbert et al., 2001)

$$\delta_{ij} = d_0 - \mathbf{r}_{ij}, \tag{A.1}$$

$$\mathbf{v}_{n_{ij}} = (\mathbf{v}_{ij} \cdot \mathbf{n}_{ij})\, \mathbf{n}_{ij}, \tag{A.2}$$

$$\mathbf{v}_{t_{ij}} = \mathbf{v}_{ij} - \mathbf{v}_{n_{ij}} - (a_i\boldsymbol{\omega}_i + a_j\boldsymbol{\omega}_j) \times \mathbf{n}_{ij}, \tag{A.3}$$

where $d = a_i + a_j$, $\mathbf{r}_{ij} = \mathbf{r}_i - \mathbf{r}_j$, $\mathbf{n}_{ij} = \mathbf{r}_{ij}/r_{ij}$, with $r_{ij} = |\mathbf{r}_{ij}|$ and $\mathbf{v}_{ij} = \mathbf{v}_i - \mathbf{v}_j$. The rate of change of the elastic tangential displacement $\mathbf{u}_{t_{ij}}$, set to zero at the initiation of a contact is

$$\frac{d\mathbf{u}_{t_{ij}}}{dt} = \mathbf{v}_{t_{ij}} - \frac{\left(\mathbf{u}_{t_{ij}} \cdot \mathbf{v}_{ij}\right) \mathbf{r}_{ij}}{r_{ij}^2}. \tag{A.4}$$

The last term in Eq. A.4 arises from the rigid body rotation around the contact point and ensures that $\mathbf{u}_{t_{ij}}$ always lies in the local tangent plane of contact. Normal and tangential forces acting on particle i are

$$\mathbf{F}_{n_{ij}} = f\left(\delta_{ij}/d\right)\left(k_n\delta_{ij}\mathbf{n}_{ij} - \gamma_n m_{eff}\mathbf{v}_{n_{ij}}\right), \tag{A.5}$$

$$\mathbf{F}_{t_{ij}} = f\left(\delta_{ij}/d\right)\left(-k_t\mathbf{u}_{t_{ij}} - \gamma_t m_{eff}\mathbf{v}_{t_{ij}}\right), \tag{A.6}$$

where $k_{n,t}$ and $\gamma_{n,t}$ are the spring stiffness and viscoelastic constants, respectively, and $m_{eff} = m_i m_j/\left(m_i + m_j\right)$ is the effective mass of spheres with masses m_i and m_j. The corresponding contact force on particle j is simply given by Newton's third law, i.e.,

$\mathbf{F}_{ji} = -\mathbf{F}_{ij}$. The function $f(\delta_{ij}/d) = 1$ is for the linear spring–dashpot model, and $f(\delta_{ij}/d) = \sqrt{\delta_{ij}/d}$ is for Hertzian contacts with viscoelastic damping between spheres.

Static friction is implemented by keeping track of the elastic shear displacement throughout the lifetime of a contact. The static yield criterion, characterized by a local particle friction coefficient μ, is modeled by truncating the magnitude of $\mathbf{u}_{t_{ij}}$ as necessary to satisfy $|\mathbf{F}_{t_{ij}}| < |\mu \mathbf{F}_{n_{ij}}|$. Thus the contact surfaces are treated as "sticking" when $|\mathbf{F}_{t_{ij}}| < |\mu \mathbf{F}_{n_{ij}}|$, and as "slipping" when the yield criterion is satisfied.

In a gravitational field $\mathbf{g}$, the translational and rotational accelerations of particles are determined by Newton's second law in terms of the total force acting on each particle i:

$$\mathbf{F}_i^{tot} = m_i \mathbf{g} + \sum_j \mathbf{F}_{n_{ij}} + \mathbf{F}_{t_{ij}} - b\mathbf{v}_i, \tag{A.7}$$

and total torques acting on each particle i:

$$\boldsymbol{\tau}_i^{tot} = -\sum_j a_i \mathbf{n}_{ij} \times \mathbf{F}_{t_{ij}}. \tag{A.8}$$

The last term $-b\mathbf{v}_i$ in the force equation represents an external damping force. This term is used to artificially enhance the energy dissipation due to two-particle contact, which is underpredicted by the MD contact force model (Luding et al., 2004). A similar damping term can also arise from the viscous drag a particle experiences due to the presence of an interstitial fluid, but that term is proportional to the relative velocity between particle and fluid.

The amount of energy lost in collisions is characterized by the inelasticity through the value of the coefficient of restitution, which is defined as the negative ratio of the particle normal velocity after collision to the velocity before collision. For the linear spring-dashpot model, the coefficient of normal restitution and contact time can be analytically obtained:

$$e_n = \exp(-\gamma_n t_c/2), \tag{A.9}$$

where the contact time t_c is given by

$$t_c = \pi\left(k_n/m_{\text{eff}} - \gamma_n^2/4\right)^{-1/2}. \tag{A.10}$$

The value of the spring constant should be large enough to avoid particle interpenetration, yet not so large as to require an unreasonably small simulation time step dt, since an accurate simulation typically requires $dt \sim t_c/50$ (Campbell, 2002). After the contact force is calculated, the equation of motion, which are ordinary differential equations, can be numerically integrated to get the particle trajectories.

APPENDIX B. VERIFICATION OF THE ORDER PARAMETER EXTRACTION

The OP is extracted from 3 DEM simulations and verified by comparing them with similar calculations of Volfson et al. (2003) for 2 DEM simulations. In Fig. B.1 the OP is plotted as a function of solid volume fraction for an inhomogeneous wall shear simulation. The OP value is averaged across the inhomogeneous direction to obtain a single value following Volfson et al. (2003). One should note that the OP reported by Volfson et al. (2003) is obtained from 2D DEM simulations, whereas the OP values reported in this work are extracted from 3D DEM simulations.

For a meaningful comparison, the reported 2D solid volume fraction is converted to the corresponding 3D solid volume fraction by using the following relation (Wachem et al., 2001)

$$\nu_{3D} = \frac{2}{\sqrt{\pi\sqrt{3}}}\nu_{2D}^{3/2}. \tag{B.1}$$

A maximum difference of about 15% is found at solid volume fraction of 0.60. Our results verify the sudden increase in the order parameter as the solid volume fraction increases from 0.60 to 0.62 that is reported in Volfson et al. (2003).

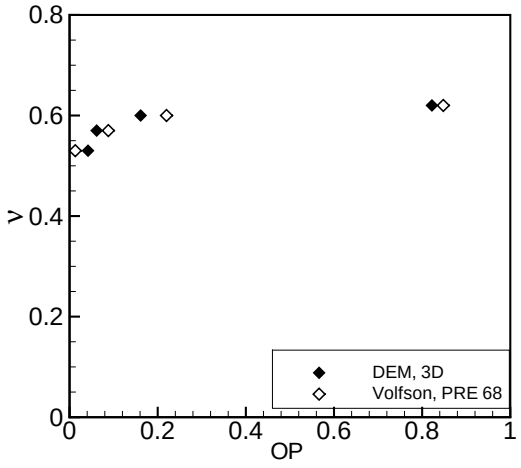

Figure B.1 Order parameter as a function of solid volume fraction for wall shear simulation. The filled symbols represent the 3D DEM data whereas blank symbols corresponds to Volfson et al. Volfson et al. (2003). Simulation parameters: $\mu_p = 0.5$, $\mu_w = 0.5$, $k^* = 10^5$ and $e = 0.7$.

BIBLIOGRAPHY

Aarons, L. and Sundaresan, S. (2006). Shear flow of assemblies of cohesive and non-cohesive granular materials. *Powder Technology*, 169:10–21.

Allen, M. P. and Tildesley, D. J. (1989). *Computer Simulation of Liquids*. Oxford: Oxford University Press.

Aranson, I. S. and Tsimring, L. S. (2002). Continuum theory of partially fluidized granular flows. *Physical Review E*, 65:061303-1–061303-20.

Bagnolds, R. A. (1954). Experiments on a gravity-free dispersion of large solid spheres in a Newtonian fluid under shear. *Proceedings of the Royal Society of London Series A: Mathematical and Physical Sciences*, 225:49–63.

Campbell, C. S. (1990). Rapid granular flows. *Annu. Rev. Fluid Mech.*, 22:57–92.

Campbell, C. S. (2002). Granular shear flows at the elastic limit. *Journal of Fluid Mechanics*, 465:261–291.

Cundall, P. and Strack, O. (1979). A discrete numerical model for granular assemblies. *Geotech*, 29:47–65.

Daerr, A. and Douady, S. (1999). Two types of avalanche behavior in granular media. *Nature*, 399:241–243.

Fenistein, D. and van Hecke, M. (2003). Kinematics-Wide shear zones in granular bulk flow. *Nature*, 425:256–256.

Gao, D., Subramaniam, S., Fox, R. O., and Hoffman, D. K. (2005). Objective decomposition of the stress tesnor in granular flows. *Physical Review E*, 71:021302-1–021302-5.

GDR MiDi group(2004). On dense granular flows. *Eur. Phys. J.E.*, 14:341–365.

Goldhirsch, I. (2003). Rapid granular flows. *Annu. Rev. Fluid Mech.*, 35:267–293.

Jaeger, H. M. and Nagel, S. R. (1992). Physics of the granular state. *Science*, 225:1523–1531.

Jaeger, H. M., Nagel, S. R., and Behringer, R. P. (1996). Granular solids, liquids, and gases. *Rev. Mod. Phys.*, 68:1259–1273.

Ji, S., Hanes, D. M., and Shen, H. H. (2009). Comparisons of physical experiment and discrete element simulatuions of sheared granular material in an annular shear cell. *Mechanics of Materials*, 41:764–776.

Johnson, P. C. and Jackson, R. (1987). Frictional Collisional Constitutive Relations for Granular Materials, with Application to Plane Shearing. *Journal of Fluid Mechanics*, 176:67–98.

Jop, P., Forterre, Y., and Pouliquen, O. (2006). A constitutive law for dense granular flows. *Nature*, 441(8):727-730.

Ketterhagen, W. R., Curtis, J. S., Wassgren, C. R., and Hancock, B. C. (2009). Predicting the flow mode from hoppers using the discrete element method. *Powder Technology*, 195:1–10.

Landau, L. D. and Lifshittz, E. M. (1980). *Statistical Physics*. Pergamon Press.

Langroudi, M. K., Turek, S., Quazzi, A., and Tardos, G. I. (2010). An investigation of frictional and collisional powder flows using a unified constitutive equation. *Powder Technology*, 197:91–101.

Lois, G., Lemaitre, A., and Carlson, M. J. (2005). Numerical test of constitutive laws for dense granular flows. *Physical Review E*, 72:051303-1–051303-16.

Losert, W., Bocquet, L., and Lubensky, T. C. and Gollub, J. P. (2000). Particle dynamics in sheared granular matter. *Physical Review Letters*, 85(7):1428-1431.

Luding, S., Hinirichsen, H., and Wolf, D. E. (2004). *The Physics of granular media*. New York: Wiley-VCH Verlag.

Lun, C. K. K., Savage, S. B., Jeffrey, D. J., and Chepuriny, N. (1984). Kinetic theories for granular flow:inelastic particles in Couette flow and slightly inelastic particles in general flow fields. *Journal of Fluid Mechanics*, 140:223-256.

Majmudar, T. S., Sperl, M., Luding, S., and Behringer, R. P. (2007). Jamming Transition in Granular Systems. *Physical Review Letters*, 98(5):058001–4.

McCarthy, J. J. and Higgs, C. F. (2009). Granular flow in a rough annular shear, validating DEM simulations with experiments. *NETL 2009 Workshop on Multiphase Flow Science*.

McCarthy, J. J., Jasti, V., Marinack, M., and Higgs, C. F. (2010). Quantitative validation of the discrete element method using an annular shear cell. *Powder Technology*, 230:70–77.

Syamlal, M., Rogers, W., and O'Brien, T. J. (1993). *MFIX Documentation: Theory Guide*. National Energy Technology Laboratory, Department of Energy.

Miller, B., Hern, C. O., and Behringer, R. P. (2003). Stress fluctuations for continuosly sheared granular materials. *Physical Review Letters*, 77(15):3110–3113.

Mueth, D. M., Jaeger, H. M., and Nagel, S. R. (1998). Force distribution in a granular medium. *Physical Review E*, 57:3164–3169.

Nasuno, S., Kudrolli, A., Bak, A., and Gollub, J. P. (2000). Time-resolved studies of stick-slip friction in sheared granular layers. *Physical Review Letters*, 58(2):2161–2171.

Nedderman, R. M. (1992). *Static and kninematics of granular material*. Cambridge: Cambridge University Press.

Plimpton, S. J. (1995). Fast parallel algorithms for short-range molecular dynamics. *Journal of Computational Physics*, 117:1–19.

Reynolds, O. (1885). On the dilatancy of media composed of rigid particles in contact. *Philos. Mag. Ser.*, 20:469–481.

Rycroft, C. H., Grest, G. S., Landry, J .W., and Bazant, M. Z. (2006). Analysis of granular flow in a pebble-bed nuclear reactor. *Physical Review E*, 74:1–16.

Savage, S. B. (1983). *Mechanics of granular materials: new models and constitutive relations*. Elsevier Ltd.

Savage, S. B. and Sayed, M. (1984). Stress developed by dry cohesionless granular materials sheared in an annular shear cell. *Journal of Fluid Mechanics*, 142:391–430.

Savage, S. B. (1998). Analyses of slow high-concentration flows of granular materials. *Journal of Fluid Mechanics*, 377:1–77.

Schaeffer, D. G. (1987). Instability in the Evolution Equations Describing Incompressible Granular Flow. *Journal of Differential Equations*, 66:19–50.

Schöllmann, S. (1999). Simulation of a two-dimensional shear cell. *Physical Review E*, 59:889-899.

Silbert, L. E., Ertas, D., Grest, G. S., Halsey, T. C., Levine, D., and Plimpton, S. J. (2001). Granular flow down an inclined plane: Bagnold scaling and rheology. *Physical Review E*, 64:051302-1–051302-13.

Srivastava, A. and Sundaresan, S. (2003). Analysis of a frictional-kinetic model for gas-particle flow. *Powder Technology*, 129:72–85.

Subramaniam, S. and Vidyapati (2009). Rheological behavior of dense granular material: DEM simulations and Order Parameter model. *NETL 2009 Workshop on Multiphase Flow Science*.

Sun, J., Battaglia, F., and Subramaniam, S. (2006). Dynamics and structures of segregation in a dense, vibrating granular bed. *Physical Review E*, 74:1–13.

Sun, J. and Sundaresan, S. (2010). A plasticity model with microstructure evolution for quasi-static granular flows. *Iutam-Isimm Symposium on Mathematical Modeling and Physical Instances of Granular flows*, 1227:280–289.

Sundaresan, S. (2001). Some outstanding questions in handling of cohesionless particles. *Powder Technology*, 115:2–7.

Syamlal, M., Guenther, C., and Pannala, S. (2009). Advanced coal gasifier designs using large-scale simulations. *Journal of Physics*, 180:1–10.

Tardos, I. T., McNamara, S., and Talu, I. (2003). Slow and intermediate flow of a frictional bulk powder in the Couette geometry. *Powder Technology*, 131:23–39.

Tsai, J. C. and Gollub, J .P. (2004). Slowly sheared dense granular flows: crystallization and nonunique states. *Physical Review E*, 70:031303-1–031303-13.

Vidyapati, Kheiripour, M., Sun, J., Sundaresan, S., Tardos, G. I., and Subramaniam, S. (2010). Experimental and computational studies of dense granular flow: transition from quasi-static to intermediate regime in a Couette shear device. *In review with Powder Technology.*

Vidyapati, Sun, J., Sundaresan, S., and Subramaniam, S. (2010). Refined Order Prameter model and its application to homogeneous shear flows. *Mannuscript in preparation.*

Volfson, D., Tsimring, L. S., and Aranson, I. S. (2003). Partially fluidized shear granular flows: Continuum theory and molecular dynamics simulations. *Physical Review E*, 68:021302-1–021302-15.

Volfson, D., Tsimring, L. S., and Aranson, I. S. (2003). Order Parameter Description of Stationary Partially Fluidized Shear Granular Flows. *Physical Review Letters*, 90(25):254301-1–254301-4.

van Wachem, B. G. M., Schaaf, J., Schouten, J. C., Krishna, R., and Bleek, C. M. (2001). Experimental validation of Langrangian-Eluerian simulations of fluidized beds. *Powder Technology*, 116:115–165.